Transfer of cGAMP into bystander cells via LRRC8 volume-regulated anion channels augments STING-mediated interferon responses and anti-viral immunity.

Zhou C., Chen X., Planells-Cases R., Chu J., Wang L., Cao L., Li Z., López-Cayuqueo K.I., Xie Y., Ye S., Wang X., Ullrich F., Ma S., Fang Y., Zhang X., Qian Z., Liang X., Cai S.Q., Jiang Z., Zhou D., Leng Q., Xiao T.S., Lan K., Yang Ji., Li H., Peng C., Qiu Z., Jentsch T.J., Xiao H.

This is the final version of the accepted manuscript. The original article has been published in final edited form in:

Immunity
2020 MAY 19 ; 52(5): 767-781
2020 APR 10 (first published online: final publication)
doi: 10.1016/j.immuni.2020.03.016

Publisher: Cell Press / Elsevier

LRRC8 volume-regulated anion channels transmit cGAMP into the bystander cells for interferon response and reinforcement of anti-viral defense

Chun Zhou,[1,16] Xia Chen,[1,2,16] Rosa Planells-Cases,[3,16] Jiachen Chu,[4] Li Wang,[1] Limin Cao,[1] Zhihong Li,[5,6] Karen I. López-Cayuqueo,[3] Yadong Xie,[1] Shiwei Ye,[7] Xiang Wang,[8] Florian Ullrich,[3] Shixin Ma,[1] Yiyuan Fang,[8] Xiaoming Zhang,[8] Zhikang Qian,[8] Xiaozheng Liang,[8] Shi-Qing Cai,[7] Zhengfan Jiang,[9] Dongming Zhou,[8] Qibin Leng,[10] Tsan S. Xiao,[11] Ke Lan,[12] Jinbo Yang,[2] Huabin Li,[13] Chao Peng,[5,6] Zhaozhu Qiu,[4,*] Thomas J. Jentsch,[3,14,*] and Hui Xiao[1,15,*]

[1]The Center for Microbes, Development and Health, CAS Key Laboratory of Molecular Virology & Immunology, Institut Pasteur of Shanghai; CAS Center for Excellence in Molecular Cell Science; University of Chinese Academy of Sciences, Chinese Academy of Sciences,
Shanghai 200031, China

[2]College of Life Sciences,
Lanzhou University,
Lanzhou, Gansu 730000, China

[3]Leibniz-Forschungsinstitut für Molekulare Pharmakologie (FMP) and Max-Delbrück-Centrum für Molekulare Medizin,
D-13125 Berlin, Germany

[4]Department of Physiology,
Johns Hopkins University School of Medicine,
Baltimore, MD 21205, USA.

[5]National Facility for Protein Science in Shanghai, Zhangjiang Lab, Shanghai Advanced Research Institute, Chinese Academy of Science,
Shanghai 201210, China.

[6]Shanghai Science Research Center, Chinese Academy of Sciences,
Shanghai 201204, China.

[7]Institute of Neuroscience and State Key Laboratory of Neuroscience, CAS Center for Excellence in Brain Science and Intelligence Technology, Chinese Academy of Sciences,
Shanghai 200031, China

[8]CAS Key Laboratory of Molecular Virology & Immunology
Institut Pasteur of Shanghai; University of Chinese Academy of Sciences, Chinese Academy of Sciences
Shanghai 200031, China

[9]Key Laboratory of Cell Proliferation and Differentiation of the Ministry of Education, School of Life Sciences, Peking University; Peking-Tsinghua Center for Life Sciences, Beijing 100871, China.

[10]Affiliated Cancer Hospital & Institute of Guangzhou Medical University, State Key Laboratory of Respiratory Diseases, Guangzhou Medical University,
Guangzhou, Guangdong 510180, China

[11]Department of Pathology, Case Western Reserve University School of Medicine, Cleveland, OH 44106, USA.

[12]State Key Laboratory of Virology,
College of Life Sciences, Wuhan University,
Wuhan, Hubei 430072, China

[13]Center for Allergic and Inflammatory Diseases & Department of Otolaryngology, Head and Neck Surgery, Affiliated Eye, Ear, Nose and Throat Hospital,
Fudan University,
Shanghai 200031, China

[14] NeuroCure Cluster of Excellence, Charité University Medicine,
D-10117 Berlin, Germany

[15]Lead contact

[16]These authors contributed equally

*Correspondence:

zhaozhu@jhmi.edu (Z.Q.), Jentsch@fmp-berlin.de (T.J.J.), huixiao@ips.ac.cn (H.X.)

SUMMARY

The second messenger cGAMP synthesized by cGAS in virus-infected or cancer cells has the potential to activate STING in bystander cells. However, the underlying mechanism and physiological relevance of the cell-to-cell cGAMP transmission remain poorly understood. Here through a candidate screen, we found that chemical blockade or genetic ablation of volume-regulated anion channels (VRACs) composed of LRRC8 heteromers resulted in defective IFN response to the DNA virus HSV-1, but not the RNA virus VSV. Biochemical and electrophysiological analyses revealed that LRRC8A/LRRC8E-containing VRACs transport cGAMP and cyclic dinucleotides across the plasma membrane. Enhancing VRAC activity by hypotonic cell swelling, cisplatin or GTPγS, TNF or IL-1, increased STING-dependent IFN response to extracellular, but not intracellular cGAMP. *Lrrc8e*$^{-/-}$ mice displayed diminished IFN response and compromised host defense to HSV-1. Our findings reveal a crucial role for LRRC8 VRACs in cGAMP cell-to-cell transmission and suggest this transmission central to anti-viral defense and vaccine development.

INTRODUCTION

The invasion and propagation of viruses and intracellular bacteria is frequently associated with the presence of double-stranded DNAs (dsDNAs) in the cytosol, which trigger diverse host defense mechanisms including the type I interferon (IFN) response (Chen et al., 2016b; Roers et al., 2016). The enzyme cyclic GMP-AMP synthase (cGAS) acts as sensor of cytosolic dsDNAs in infected and malignant cells (Sun et al., 2013). Upon binding to dsDNA, cGAS catalyzes the formation of 2'3'cGMP-AMP (cGAMP) (Ablasser et al., 2013a; Chen et al., 2016b; Wu et al., 2013), a second messenger that directly binds to the ER-anchored adaptor protein Stimulator of interferon genes (STING; also referred to as MITA or ERIS) (Ishikawa and Barber, 2008; Sun et al., 2009; Zhong et al., 2008). Subsequently, STING triggers the activation of the kinase TBK1, which then phosphorylates the transcriptional factor IRF3 to induce a robust IFN response (Ablasser and Chen, 2019; Ablasser and Hur, 2020; Barber, 2015; Wu et al., 2013). cGAMP is uniquely produced in metazoans; however, other types of cyclic dinucleotides (CDNs) such as c-di-AMP (cdA), c-di-GMP (cdG) and 3'3'cGAMP, are produced by a wide array of prokaryotes and can also activate STING to elicit IFN responses (Danilchanka and Mekalanos, 2013; Margolis et al., 2017). cGAMP produced in virus-infected cells (Ablasser et al., 2013b) or cancer cells (Chen et al., 2016a) can also be transmitted into bystander cells through gap-junctions, triggering an IFN response therein. cGAMP packaged into viral particles can be transferred into newly infected cells as well (Bridgeman et al., 2015; Gentili et al., 2015). Moreover, the folate transporter Slc19a1 has been implicated in the transport of extracellular cGAMP into the cytosol of a subset of human cells (Luteijn et al., 2019; Ritchie et al., 2019).

The volume-regulated anion channel (VRAC) controls cell volume by releasing Cl^- and organic osmolytes in response to cell swelling (Hoffmann et al., 2009; Jentsch, 2016; Osei-Owusu et al., 2018; Pedersen et al., 2016), and consists of a heteromer of LRRC8 proteins (Qiu et al., 2014; Voss et al., 2014). In addition to the obligatory subunit

LRRC8A (also known as SWELL1), at least one of the other LRRC8 isoforms (LRRC8B, -C, -D or -E) is needed to form hetero-multimeric channels in the plasma membrane (Voss et al., 2014). LRRC8 channels (VRACs) not only conduct Cl^- and other halide ions, but also a variety of organic molecules. These include taurine (Qiu et al., 2014; Voss et al., 2014), inositol, glutamate and other neurotransmitters (Lutter et al., 2017; Yang et al., 2019), and therapeutic agents such as cisplatin and carboplatin (Planells-Cases et al., 2015) and blasticidin S (Lee et al., 2014). Whereas all LRRC8A-containing heteromers yield swelling-activated Cl^- currents, the transport of organic compounds depends on VRAC's subunit composition. Inclusion of LRRC8D enhances the transport of all tested organic substrates (Lutter et al., 2017; Planells-Cases et al., 2015), whereas inclusion of LRRC8E rather specifically stimulates the transport of the negatively charged glutamate and aspartate (Lutter et al., 2017). VRACs are thought to be important for diverse processes including insulin secretion (Best et al., 2010; Kang et al., 2018; Stuhlmann et al., 2018), neuron-glia interaction (Yang et al., 2019), stroke (Wilson et al., 2019; Yang et al., 2019), apoptosis and cancer drug resistance (Planells-Cases et al., 2015), and sperm cell development (Luck et al., 2018). The importance of VRAC is further illustrated by the multiple tissue abnormalities and lethality of *Lrrc8a*-deficient mice (Kumar et al., 2014; Platt et al., 2017). Besides activation by cell swelling, VRACs can be slowly opened by pro-apoptotic drug cisplatin (Planells-Cases et al., 2015), GTPγS, and certain G-protein coupled receptors (Hoffmann et al., 2009; Nilius et al., 1999; Voets et al., 1998).

Here we examined the roles of anion channels in anti-viral defense. A candidate screen revealed that inhibition of VRAC resulted in increased viral propagation upon HSV-1 infection. *Lrrc8a*$^{-/-}$ cells exhibited higher viral loads after HSV-1 infection, but not VSV infection indicating a difference in responses to DNA versus RNA virus. The STING pathway activated by extracellular cGAMP was dampened in *Lrrc8a*$^{-/-}$ or *Lrrc8e*$^{-/-}$ cells and further biochemical analyses revealed transport of cGAMP and CDNs across the plasma membrane by VRACs containing LRRC8A and -E. Our findings suggest that

this transport is central to the host control of HSV-1 infection, likely through the induction of reinforcing IFN-β synthesis in distant bystander cells.

RESULTS

LRRC8 VRACs Play a Crucial Role in Anti-viral IFN Response

To explore the role of anion channels in anti-viral defense, we screened a small library of anion channel inhibitors using a cell-based viral infection platform modified from our previous study (Du et al., 2015). Infection with herpes simplex virus KOS strain (HSV-1) causes necrotic cell death in murine embryonic fibroblasts (MEFs) (Wang et al., 2014), a process often inversely correlated with IFN response. As proof-of-principle, *Sting*$^{-/-}$ MEFs underwent necrotic cell death following HSV-1 infection (Figure S1A). The screen revealed that 4-(2-Butyl-6,7-dichloro-2-cyclopentyl-indan-1-on-5-yl) oxobutyric acid (DCPIB) and carbenoxolone (CBX), two well-known VRAC inhibitors (Benfenati et al., 2009; Decher et al., 2001), augmented necrotic cell death (Figure 1A) and viral propagation (Figure S1B) following HSV-1 infection. Conversely, other anion channel blockers, including CaCCinh-A01, DIDS and glibenclamide, lacked a notable impact on HSV-1-induced cellular pathology (Figures 1A). Interestingly, treatment with DCPIB efficiently suppressed the IFN response to the DNA virus HSV-1 (Figures 1B and S1C), but had no significant impact on the induction of *Ifnb* and *Cxcl10* by RNA virus vesicular stomatitis virus (VSV) (Figure 1C). These results suggested VRAC as a potential modulator of the IFN response to DNA virus.

As DCPIB and CBX are non-specific VRAC inhibitors and can, for instance, also block other channels such as pannexin-1 and connexins (Ablasser et al., 2013b; Friard et al., 2017), we employed a genetic approach to validate a role of VRAC in anti-viral IFN response. Whereas RNAi of *Cx43* or *Panx1* failed to affect the HSV-1-induced IFN response, RNAi of *Lrrc8a* severely compromised the induction of *Ifnb* and *Cxcl10* (Figure S1D). To rigorously examine the role of LRRC8 VRACs in anti-viral defense, we disrupted the obligatory Lrrc8a subunit in L929 mouse fibroblasts by Crispr-cas9

technology. *Lrrc8a*$^{-/-}$ L929 cells exhibited blunted expression of *Ifnb* and *Cxcl10* at both mRNA (Figures 1D) and protein levels (Figure 1E). Following VSV infection, however, both wild-type (WT) and *Lrrc8a*$^{-/-}$ L929 cells elicited robust IFN response (Figure 1F) and exhibited a similar viral load (Figure 1G). Conversely, increased viral loads were associated with *Lrrc8a*-deficiency following HSV-1 infection (Figure 1G). Together, these results uncovered a role for LRRC8 VRACs in the IFN response for host defense against DNA viruses.

LRRC8A/E-containing VRACs Promote Anti-viral IFN Response

We next sought to extend the role of LRRC8A in anti-viral response to various primary cells. First, WT and *Lrrc8a*$^{-/-}$ MEFs (Figure 2A) were created by transduction of control or Cre-expressing retroviral vector to primary MEFs isolated from *Lrrc8a*$^{f/f}$ mice (Yang et al., 2019). Upon HSV-1 infection, *Lrrc8a*$^{-/-}$ MEFs showed diminished expression of *Ifnb* and interferon stimulated genes (Isgs) *Cxcl10* and *Mx2* (Figure 2B). Moreover, *Lrrc8a*$^{-/-}$ MEFs produced less amounts of IFN-β and CXCL-10 in response to HSV-1, but not VSV infection (Figure S2A). Next, WT and *Lrrc8a*$^{-/-}$ mouse lung fibroblasts (MLFs) and bone marrow-derived macrophages (BMDMs) were generated from tamoxifen-treated *Lrrc8a*$^{f/f}$ and *Lrrc8a*$^{f/f:creERT}$ mice, respectively. Upon HSV-1 infection, *Lrrc8a*$^{-/-}$ MLFs showed markedly reduced IFN responses (Figures 2C and S2B), which were correlated with increased expression of the HSV-1 encoded genes LAT and gB (Figure 2D). Likewise, *Lrrc8a*$^{-/-}$ BMDMs showed impaired *Ifnb* responses to HSV-1, but not to VSV infection (Figures 2E and S2C). Hence Lrrc8a participates in the anti-HSV defense in a wide range of cell types, including immune and non-immune cells.

Next, we generated mice deficient in each other subunit (*Lrrc8b*, *Lrrc8c*, *Lrrc8d* and *Lrrc8e*) to identify which one is needed, together with Lrrc8a, for anti-viral IFN response. *Lrrc8e*-deficiency markedly reduced HSV-1-triggered IFN response whereas deleting *Lrrc8b*, *Lrrc8c* or *Lrrc8d* lacked a significant impact (Figure 2C). Further, MLFs deficient in *Lrrc8e*, but not *Lrrc8b-d*, showed heightened viral replication upon

HSV-1 infection (Figure 2D). Furthermore, in BMDMs, *Lrrc8e*-deficiency compromised HSV-1-induced IFN response, particularly at lower MOI of viral infection (Figures 2F and S2D). Like *Lrrc8a*$^{-/-}$ BMDMs (Figure 2E), *Lrrc8e*$^{-/-}$ BMDMs displayed a normal IFN response to VSV infection (Figures 2F and S2D). Genetic deletion or RNAi of *Lrrc8e* in L929 cells also severely disrupted IFN responses to HSV-1 infection (Figures S2E and S2F). Hence incorporation of the Lrrc8e subunit into the Lrrc8a-containing heteromeric VRACs is crucial for their role in anti-viral IFN response.

LRRC8A/E-containing VRACs Enhance Extracellular cGAMP-induced STING Activation

To understand how LRRC8A/E VRACs regulate anti-viral IFN responses, we examined the corresponding signaling in WT and VRAC-deficient cells. In WT MEFs, both HSV-1 and VSV infection robustly activated TBK1 and IRF3 as evident from markedly increased phosphorylation, also STAT1 whose phosphorylation dependent on a feedback response by autocrine or paracrine IFN (Figures 3A and S3A). *Lrrc8a*-ablation reduced the phosphorylation of TBK1, IRF3 and STAT1 upon infection with HSV-1, but not VSV in MEFs (Figures 3A and S3A). Because HSV-1 primarily engages the cGAS/STING pathway, whereas VSV predominantly acts through RIG-I/MAVS, we reasoned that LRRC8/VRACs might impinge on cGAS/STING signaling. However, directly activating cGAS by transfection of interferon stimulating DNA (ISD) triggered similar TBK1 and IRF3 activation in WT and *Lrrc8a*$^{-/-}$ (Figure 3B) or *Lrrc8e*$^{-/-}$ MEFs (Figure S3B). Likewise, transfecting cGAMP into the cytosol to directly activate STING resulted in similar phosphorylation of TBK1, IRF3 and STAT1 in WT and *Lrrc8a*$^{-/-}$ cells (Figure 3B). Hence, whereas VRACs are important for activating STING-dependent signaling upon HSV-1 infection, they do not influence the signaling events elicited by cytosolic agonists of cGAS or STING. Similar cGAMP production in WT and *Lrrc8a*$^{-/-}$ cells upon HSV-1 infection (Figure S3C) excluded a role for VRACs in cGAMP synthesis.

Given VRAC's ability to transport metabolites and drugs, we wondered whether VRACs may transport cGAMP from infected cells to bystander cells where it may elicit an additional IFN response through STING. To indirectly measure cGAMP uptake though VRACs, we added cGAMP to culture media without transfection reagent and measured the induced IFN responses. Despite being hydrophilic and hence poorly permeable through lipid bilayers, extracellular cGAMP triggered marked phosphorylation of TBK1 and IRF3 in WT MEFs (Figure 3C). Similar effects were observed with extracellularly added bacterial cdA and 3'3'cGAMP (Figures 3C and S3D). Importantly, added cGAMPs and cdA induced much less phosphorylation on TBK1 and IRF3 in *Lrrc8a*$^{-/-}$ MEFs (Figures 3C and S3D). Also with MLFs, added cGAMP strongly induced *Ifnb* and *Cxcl10* expression, but much less in *Lrrc8a*$^{-/-}$ cells (Figure 3D). Mirroring the roles of Lrrc8a and Lrrc8e in response to HSV-1 infection, ablation of *Lrrc8e*, but not of *Lrrc8b*, *-c* or *-d*, significantly reduced the IFN response to cGAMP extracellularly added to MLFs (Figure 3D). *Lrrc8e*-deficiency also impaired the secretion of CXCL-10 and CCL-5 in response to extracellular, but not to transfected cGAMP, nor to the cell permeable STING agonist DMXAA, LPS or polyI:C (Figure 3E). Consistently, extracellular cGAMP induced less IFN-β production in *Lrrc8a*$^{-/-}$ BMDMs (Figure 3F) or MLFs (Figure S3E). These results indicate that Lrrc8a/e-containing VRACs may have a role in transporting cGAMP through the plasma membrane.

The notion that Lrrc8e-containing VRACs mediate cGAMP transport was further buttressed by direct measurements of cellular cGAMP uptake using liquid chromatography-mass spectrometry (LC-MS) (Figure 3G). Ablation of either *Lrrc8a* or *Lrrc8e*, but not of *Lrrc8b-d*, decreased uptake of cGAMP into the cytosol by roughly 60% (Figure 3G). Collectively, these data strongly suggest that Lrrc8e-containing VRACs may operate as a cell membrane conduit for cGAMP entry. With its larger size, extracellularly added FITC-conjugated cGAMP was unable to trigger *Ifnb* and *Cxcl10*

expression (Figure S3F) or induce IRF3 phosphorylation (Figure S3G), although it elicited robust TBK1/IRF3 phosphorylation when transfected with liposome (Figure S3H).

The Response to Extracellular cGAMP Depends on VRAC Channel Activity

If cGAMP permeates through VRAC's ion conducting pore, the cellular effects of externally added cGAMP are expected to be similarly affected by procedures that block or enhance VRAC-mediated Cl^- currents. Indeed, VRAC blockade with DCPIB or CBX diminished extracellular cGAMP-induced *Ifnb* and *Cxcl10* expression in peritoneal macrophages (pMs) (Figure 4A) and MLFs (Figures 4B and 4C). Whereas DCPIB inhibited the uptake of extracellular cGAMP in WT cells by roughly 60%, it did not affect uptake into *Lrrc8a*$^{-/-}$ or *Lrrc8e*$^{-/-}$ cells (Figure 4D). Conversely, DCPIB lacked significant impact on IFN responses to LPS, polyI:C or IFN-β (Figures S4A, S4B, and S4C). Hence, cellular effects of extracellular cGAMP are impaired when VRAC's ion-conducting pore is blocked.

By contrast, GTPγS and cisplatin, two agents capable of potentiating VRAC activity (Planells-Cases et al., 2015; Voets et al., 1998), markedly enhanced extracellular cGAMP-induced IFN response in MLFs, BMDMs and L929 cells (Figures 4E, 4F, and S4D). As expected, GTPγS- or cisplatin-enhanced cGAMP response was abrogated in *Lrrc8a*$^{-/-}$ or *Lrrc8e*$^{-/-}$ cells (Figures 4E, 4F, and S4D). Strikingly, hypotonic cell swelling, the most potent stimulus for opening VRACs, greatly enhanced cGAMP-induced IFN responses in various mouse primary cells (MLF, pM and MEF) (Figures 4G, 4H, and S4E) and human cells (HeLa and THP-1) (Figures S4F and S4G). Collectively, these data strongly support the notion that cGAMP permeates VRAC's pore.

Hypotonic Activation of VRACs Enhances the Entry of Extracellular cGAMP

While cell swelling robustly enhanced the IFN response to extracellular cGAMP, it failed to augment responses to intracellularly delivered cGAMP (Figure S5A). It neither

potentiated LPS-, polyI:C- or IFN-β-induced gene expression (Figures S5B and S5C). Cell swelling-promoted IFN responses to extracellular cGAMP were markedly reduced in *Lrrc8a*$^{-/-}$ L929 and MEFs (Figures 5A, 5B, and S4E), and in L929 or BMDM lacking *Lrrc8e* (Figures 5A and 5C). In contrast, Lrrc8b, -c, -d apparently lacked a significant role in cell swelling-promoted cGAMP response (Figure S5D). Likewise, RNAi of *Panx1* or *Cx43* did not affect the response to extracellular cGAMP in the setting of cell swelling (Figure S5E).

In contrast to hypotonic swelling, exposure to hypertonic medium did not influence extracellular cGAMP-induced IFN response (Figure S5F). Hypotonicity-boosted *Ifnb* expression was abrogated by DCPIB, but not by glibenclamide or CaCCinh-A01, excluding the involvement of several other Cl^- channels (Figure 5D). Cellular depletion of Cl^- did not abolish the effect of hypotonicity on the extracellular cGAMP response, suggesting Cl^- efflux is not required for cGAMP transport (Figure 5E). Cell swelling augmented extracellular cGAMP-elicited IRF3 phosphorylation, which was contingent on the expression of Lrrc8a or Lrrc8e in various cell types including MEF (Figure 5F), BMDM (Figure S5G), L929 (Figure S5H) and HeLa (Figure S5I).

Under hypotonic condition, bacterial cdA, cdG and 3'3'cGAMP also induced robust IFN responses, which were severely diminished in *Lrrc8e*-RNAi cells (Figure 5G). Finally, we measured cGAMP entry by LC-MS in response to osmotic cell swelling. Hypotonicity profoundly enhanced cGAMP entry into cells (Figure 5H), a process that was strongly inhibited by DCPIB (Figure 5H) or genetic ablation of *Lrrc8a* or *Lrrc8e* (Figure 5I). Together, these data support a central role for Lrrc8e-containing VRACs in transporting cGAMPs and CDNs.

LRRC8A/E-containing VRACs Transmit cGAMP to Bystander Cells

Upon HSV-1 infection, cGAMP was detected in MEFs (Figure 6A), which were all viable (Figure S6A), and in the surrounding medium (Figure 6B), as quantified by LC-

MS and more sensitive ELISA (Gentili et al., 2019), respectively. Heat-inactivated media from HSV-1-infected WT MEFs induced *Ifnb* expression in WT, but not *Lrrc8a*$^{-/-}$ recipient cells, in a Sting-dependent but cGas-independent manner (Figure 6C). Preincubation with snake venom phosphodiesterase I (SVPDE), a cGAMP hydrolase (Ablasser et al., 2013b) abrogated the ability of culture media from HSV-1-infected cell to induce IFN response (Figure S6B). Media collected from HSV-1-infected *Lrrc8a*$^{-/-}$ cells showed less cGAMP (Figure 6B) or reduced capacity to trigger *Ifnb* than those from HSV-1-infected WT cells (Figure S6C), although their intracellular cGAMP productions were comparable (Figure S3C). Hence, VRAC probably mediates not only the uptake, but also the export of cGAMP.

In addition to HSV-1, adenovirus (Lam et al., 2014) and murine cytomegalovirus (MCMV) (Bridgeman et al., 2015; Stempel et al., 2019) also engage the cGAS/STING pathway to mount IFN response. Both adenovirus and MCMV propagated more efficiently in *Lrrc8a*$^{-/-}$ MEFs than WT controls (Figure 6D), suggesting a more general role for VRAC in the host defense against DNA viruses. We then tested whether cGAMP produced by DNA virus-infected cells could activate STING in bystander cells, using the formation of perinuclear STING aggregates as read-out for STING activation by cGAMP (Ishikawa et al., 2009; Luo et al., 2016) (Figure S6D). We used adenovirus-GFP to infect WT or *Lrrc8a*$^{-/-}$ MEFs that were transiently transfected with a STING-cherry plasmid. After low MOI infection, cells infected with adenovirus-GFP exhibited prominent green fluorescence and STING-cherry aggregates (Figure 6E). STING-cherry aggregates were also detected in uninfected cells identified by the absence of green fluorescence. These cells were often physically separated from infected cells (Figure 6E). In *Lrrc8a*$^{-/-}$ MEFs, STING aggregates were much less prominent in distant uninfected cells (Figure 6E).

To further test whether cGAMP can be transmitted through VRACs from infected cells to bystander cells, we co-cultured HSV-1 pre-infected cells with uninfected bystander

WT or *Lrrc8a*$^{-/-}$ MEFs separated by a transwell filter for 6 h. We then measured the IFN response in the bystander cells. Remarkably, while physically separated, bystander WT, but not *Lrrc8a*$^{-/-}$ cells showed IFN induction (Figure 6F). While bystander IFN response was abolished in *Sting*$^{-/-}$ cells, a considerable induction of *Ifnb* was detected in *Cgas*$^{-/-}$ cells (Figure S6E). The moderate reduction in IFN response observed in *Cgas*$^{-/-}$ bystander cells (Figures S6E and 6C) might be attributable to an unexpected role of cGAS in the extracellular cGAMP response (Liu et al., 2019). Importantly, inclusion of DCPIB (Figure S6E) during the co-culture diminished IFN response in WT, but not *Lrrc8a*$^{-/-}$ recipients. Unlike HSV-1-infected cells, VSV-infected cells did not trigger significant *Ifnb* expression in transwell-separated bystander cells (Figure S6F). We also investigated the transmission of cGAMP from donor cells in which cGAMP synthesis was not stimulated by infection, but rather by transfection with DNA or overexpression of cGAS. These cells also induced marked Lrrc8a- and Sting-dependent IFN induction in bystander cells (Figure 6G). Hence, cGAMP can be transmitted to bystander cells to elicit a reinforcing IFN response.

To test whether cGAMP can directly pass through VRAC channel pores, we performed whole-cell patch-clamp recordings. Intracellular Cl^- was replaced with equal concentration of $cGAMP^{2-}$ as the only permeant anion and VRACs were activated by perfusion of hypotonic bath solution. The negatively charged cGAMP carried small but notable inward currents representing $cGAMP^{2-}$ efflux from WT HeLa (Figure 6H) and HCT116 (Figure S6G) cells. The leftward shifts in reversal potential indicated that the cGAMP permeability of VRAC is significant, although less than that of Cl^- (estimated P_{cGAMP}/P_{Cl}: ~0.1 assuming all intracellular cGAMP as free divalent anions) (Figure 6I). The cGAMP-mediated inward currents were abolished in *LRRC8A*$^{-/-}$ HeLa cells (Figures 6H, 6J, and 6K) and were blocked by DCPIB (Figure S6G). Notably, the VRAC Cl^- currents were not blocked by extracellular 200 μM cGAMP (Figure S6H). These data strongly support VRAC as a direct conduit for cGAMP.

LRRC8A/E-containing VRACs Facilitate the Host Defense against HSV-1

Contrasting with severely affected *Lrrc8a*$^{-/-}$ mice (Kumar et al., 2014), *Lrrc8e*$^{-/-}$ mice were viable and lacked an obvious phenotype. We intravenously infected *Lrrc8e*$^{-/-}$ mice and their control littermates with HSV-1. WT mice rapidly launched a robust IFN response, secreting large amounts of IFN-β, CXCL-10, CCL-5, and TNF into the bloodstream 24 h post-infection (Figure 7A). In contrast, *Lrrc8e*$^{-/-}$ mice had severely compromised response to HSV-1 infection, showing marked reduction in IFN-β, CXCL-10, CCL-5 and TNF (Figure 7A). Moreover, compared to WT mice, expression levels of *Ifnb*, *Cxcl10* and *Ccl5* were considerably lower in the lung and liver tissues of *Lrrc8e*$^{-/-}$ mice (Figure 7B). Viral gene expression was increased in multiple tissues of *Lrrc8e*$^{-/-}$ mice (Figure 7C), correlating with heightened viral loads in the liver and kidney of *Lrrc8e*$^{-/-}$ mice (Figure 7D). Consequently, *Lrrc8e*$^{-/-}$ mice displayed much more severe morbidity and greater weight loss than WT mice throughout the course of infection (Figure 7E). Notably, following VSV infection for 24 h, both WT and *Lrrc8e*$^{-/-}$ mice produced similar amounts of IFN-β, CXCL-10 and TNF in their sera (Figure S7A). We conclude that Lrrc8e-containing VRACs play a crucial role in host defense against DNA virus HSV-1 *in vivo*.

Considering a crucial role for VRAC in anti-viral IFN response, we wondered whether VRAC-mediated cGAMP transmission could be enhanced by inflammation. We screened cytokines and growth factors for their ability to influence the IFN response to extracellular cGAMP. The cytokine TNF enhanced extracellular cGAMP-induced *Ifnb* expression in BMDMs (Figure S7B). Notably, TNF by itself neither raised intracellular cGAMP-induced *Ifnb* expression nor exerted a notable effect in *Lrrc8a*$^{-/-}$ BMDMs (Figure S7C). While being ineffective in BMDMs, IL-1β markedly increased extracellular cGAMP-induced response in MEFs, as did TNF (Figure S7D). IL-1β's effect likewise depended on the extracellular presence of cGAMP, and functional VRAC channels (Figures S7D and S7E). Measurement of cGAMP uptake confirmed

that TNF and IL-1β enhanced cGAMP transport through VRACs (Figure S7F), suggesting VRACs as both an effector and a propagator of inflammation.

DISCUSSION

Here we found that volume-regulated LRRC8 VRACs were critically involved in the host defense against DNA viral infection by transporting cGAMP across plasma membrane. Promotion of cGAMP-STING-dependent IFN responses in distant bystander cells may provide support to the infected cells. Our findings also suggest that cGAMP transmission through VRACs can be boosted by a diversity of stimuli including cell swelling, anti-cancer drugs and cytokines.

The cGAS-STING pathway has the capacity to launch robust IFN responses, but highly pathogenic viruses often dampen or cripple this pathway. For example, HSV-encoded ICP27 can interfere with TBK1 activation and thereby prevent virus-infected cells from producing IFN response (Christensen et al., 2016). The host must evolve effective countermeasures, and bystander immune activation has emerged as an effective mechanism for thwarting viral immune evasion (Holmgren et al., 2017). cGAMP can be transported to neighboring cells via gap-junctions (Ablasser et al., 2013b) or Slc19a1 (Luteijn et al., 2019; Ritchie et al., 2019). We discovered a role for VRACs as a conduit for transporting cGAMP into bystander cells in which it reinforces the STING-dependent IFN response. Whereas gap-junctions only allow cGAMP transmission between physically connected cells, VRACs may facilitate the transfer of cGAMP into distant bystander cells, thereby reaching a larger number of cells. Only a subset of human cells exhibit Slc19a1-dependent cGAMP uptake, which was not seen in several mouse cell types tested (Luteijn et al., 2019). Likewise, we found that different cell types from both human and mouse exhibited variable VRAC-mediated cGAMP transport. Notably, while Lrrc8e-containing VRACs did not directly affect cGAMP production or cGAMP-triggered STING activation in virus-infected cells, ablation of *Lrrc8e* in mice resulted in compromised IFN response and ineffective defense against

HSV-1 infection, thus supporting the notion that cGAMP transmission to the bystander cells as an effective countermeasure to DNA viral infection. Ablation of *Lrrc8a*, which totally abolishes VRAC activity, inhibited cGAMP uptake by only ~50-70% in a wide range of cell lines and primary cells. The remainder may reflect the transport activity of the plasma membrane folate transporter Slc19a1 (Luteijn et al., 2019; Ritchie et al., 2019), P2X7 purinergic receptors (Zhou et al., 2020) or yet to be identified transporters (Liu et al., 2019). LRRC8 VRACs may work in concert with these transporters to conduct cGAMP and CDNs in a cell type- and context-dependent manner.

LRRC8 VRACs are largely, but probably not completely closed under resting conditions. Indeed, VRAC-mediated transport of cisplatin (Planells-Cases et al., 2015) or glutamate (Yang et al., 2019) can occur without opening VRAC with hypotonic swelling or other stimuli. We found that VRACs transported cGAMP also under resting conditions and that this transport could be stimulated further by hypotonic cell swelling, cisplatin or GTPγS, or TNF or IL-1. Given that ROS-promoted cysteine oxidation can enhance LRRC8 VRACs (Gradogna et al., 2017; Varela et al., 2004), VRACs may be further activated during viral infection by factors such as TNF, IL-1 or ROS. VRACs transport a broad spectrum of small organic compounds contingent on their LRRC8 subunit composition (Lee et al., 2014; Lutter et al., 2017; Planells-Cases et al., 2015). Whereas LRRC8A complexes with either one of LRRC8B-E to conduct Cl^- efflux, inclusion of LRRC8D enabled the transport of all investigated organic compounds (Lutter et al., 2017). Our results indicate that LRRC8A/E-containing VRACs are particularly important for the transport of cGAMP and CDNs. Although the principles governing the substrate specificity of LRRC8 channels remain unclear, it is noteworthy that negatively charged aspartate could not only be transported by LRRC8D-containing VRACs, but also by VRACs containing LRRC8E or LRRC8C (Lutter et al., 2017; Schober et al., 2017). The fact that cGAMP is negatively charged points to a more general role of LRRC8E-containing VRACs in transporting negatively charged compounds. The relative expression of LRRC8B, -C, -D, -E, as well as cell-intrinsic

regulatory networks, likely influence cell type-specific roles of VRAC and the importance of specific LRRC8 subunits in cGAMP transport.

Being channels, VRACs transport substrates by passive diffusion along their electrochemical gradients. Hence, they may mediate both cellular efflux and uptake of cGAMP. This concept is supported by our observation that more cGAMP was exported by HSV-infected WT cells than *Lrrc8a*$^{-/-}$ cells. The negative charges of cGAMP, together with the concentration gradient, would provide a driving force for cGAMP exit from cells. Likewise, under appropriate cGAMP concentration gradients, VRACs can mediate cGAMP uptake as demonstrated by equilibrium potential calculations (not shown). Conceivably, other mechanisms of cGAMP release might also come into play during HSV-1 infection, including Slc19a1 and RIPK3-MLKL-mediated formation of pro-necrotic pores (Su et al., 2014; Wang et al., 2014).

The role of LRRC8 VRACs in immunity may extend well beyond infections with DNA viruses. Being capable of transporting bacterial CDNs, VRACs may also play a role in shaping immune responses against bacterial pathogens. Tumor-derived cGAMP can be transported into host cells, where it elicits IFN response to augment NK cell activation (Marcus et al., 2018). Hence, it is tempting to speculate that VRAC-mediated cGAMP efflux and/or influx might also have a role in these processes. Our work suggests that it might be worthwhile to test the role of VRACs in vaccination and explore the possibility of using VRAC agonists as co-adjuvant for cGAMP in cancer vaccine.

In conclusion, we found a role for LRRC8/VRAC-mediated cGAMP transmission in host defense, likely by alerting distant bystander cells to trigger an effective anti-viral IFN response. The demonstration of an interplay between cell volume regulation and innate immune response and the cooperation among infected cells and non-infected cells in host defense may have profound implications in infection, cancer and vaccine development.

ACKOWLEDGEMENTS

This study was supported by the Key development and research project 2016YFA0502100; the Key Cooperation Program of International Partnership Program (153831KYSB20180003), the Strategic Priority Research Program (XDB29030302), and the External Cooperation Program (153211KYSB20160001) of the Chinese Academy of Sciences; National Natural Science Foundation of China grants (81720108019, 81725004 and 31700784); the Shanghai Municipal Science and Technology Major Project (2019SHZDZX02); the Joint Research grant with State Key Laboratory of Microbial Metabolism, School of Life Science and Biotechnology, Shanghai Jiao Tong University (MMLKF16-11) to CP; and the European Research Council Advanced Grant 740537 (VolSignal) to TJJ.

AUTHOR CONTRIBUTIONS

C.Z., X.C. and H.X. conceived and designed the research; C.Z., X.C., R.P-C., J.C., L.W., L.C., Z.L., K.I.L-C., Y.X., S.Y., T.L., X.W., F.U., S.M., and Y.F. performed experiments; X.Z., Z.Q., X.L., S.C., Z.J., Q.L., D.Z., T.S.X., K.L., J.Y., H.L., and C.P. provided materials and technical support; Z.Q., T.J.J., and H.X. supervised the study; C.Z., X.C., Z.Q., T.J.J., and H.X. wrote the paper.

DECLARATION OF INTERESTS

The authors declare no competing interests.

FIGURE LEGENDS

Figure 1. VRAC Blockade Impairs HSV-induced IFN Responses.

(A) MEFs pretreated with various chloride channel inhibitors (CaCCinh-A01 (15 μM), DIDS (60 μM), glibenclamide (30 μM), CBX (100 μM), DCPIB (20 μM)) were infected with HSV-1 (MOI: 0.01) for 36 h, and then fixed and stained with 0.5% crystal violet for 2 h.

(B, C) MEFs pretreated with 20 μM DCPIB were infected with HSV-1 (MOI: 0.01) (B) or VSV (MOI: 0.01) (C) for 12 h. RT-PCR was conducted to assess *Ifnb* and *Cxcl10* expression (n=3 biological replicates).

(D-F) L929 cells were uninfected (UI) or infected with HSV-1 (D, E) or VSV (F) for 12 h. The IFN responses were assessed by RT-PCR (D, F) or ELISA (E) (n=3 biological replicates).

(G) L929 cells were uninfected or infected with HSV-1 (MOI: 0.1) or VSV (MOI: 0.01) for 24 h. The viral titers were measured by plaque assay (n=3 biological replicates).

Data are presented as mean ± SEM (*p<0.05, **p<0.01, ***p<0.001, ns: not significant; analyzed by Student's *t* test).

See also Figure S1.

Figure 2. LRRC8A/E-containing VRACs increase HSV-1-induced IFN responses.

(A, B) Primary WT and *Lrrc*8a$^{-/-}$ MEFs confirmed by immunoblotting (A) were infected with HSV-1 for 9 h, and the expression of *Ifnb* and *Cxcl10* were quantified by RT-PCR (B, n=3 biological replicates).

(C, D) MLFs were uninfected or infected with HSV-1 (MOI: 0.5) for 9 h, and the expression of *Ifnb* and Isgs (C), as well as viral genes (D) were quantified by RT-PCR (n=3 biological replicates).

(E, F) BMDMs were infected with HSV-1 or VSV (MOI: 0.1 for (E), and 0.1 or 1 for (F)) for 9 h, the expression of *Ifnb* was quantified by RT-PCR (n=3 biological replicates).

Data are presented as mean ± SEM (*p<0.05, **p<0.01, ***p<0.001 and ns: not significant; analyzed by Student's *t* test).

See also Figure S2.

Figure 3. LRRC8A/E-containing VRACs Facilitate Extracellular cGAMP, but not Intracellular cGAMP-induced IFN Responses.

(A-C) MEFs were treated with HSV-1 (MOI: 0.5) (A), cGAMP (2 μg/ml) or ISD (1 μg/ml) transfected with lipofectamine 2000 (B), or cGAMP (10 μg/ml) or cdA (10

μg/ml) added to media (C) for 3 h. The activation of STING signaling was assessed by immunoblotting. Data are representative of four independent experiments.

(D) MLFs were stimulated with added cGAMP (5 μg/ml) for 6 h. The expression of *Ifnb* and *Cxcl10* was quantified by RT-PCR (n=3 biological replicates).

(E) MLFs were stimulated with cGAMP (5 μg/ml), polyI:C (10 μg/ml), LPS (100 ng/ml), DMXAA (5 μM), or lipofectamine-transfected cGAMP (2 μg/ml) or polyI:C (1 μg/ml) for 18 h. The secretion of chemokines was measured by ELISA (n=3 biological replicates).

(F) BMDMs were treated with cGAMP (5 μg/ml) for 12 h, and the secreted IFN-β was measured by ELISA (n=3 biological replicates).

(G) MLFs were treated with cGAMP (2 μg/ml) for 1 h, and the cytosolic cGAMP was quantified by LC-MS (n=3 biological replicates).

Data are presented as mean ± SEM (*p<0.05, **p<0.01, ***p<0.001, ns: not significant; analyzed by Student's *t* test). UT: untreated.

See also Figure S3.

Figure 4. VRAC Channel Activity Positively Correlates with Extracellular cGAMP Responses.

(A) pMs were stimulated with 5 μg/ml cGAMP for 3 h in the presence of various amounts (5-80 μM) of DCPIB or 100 μM CBX. The expression of *Ifnb* was measured by RT-PCR (n=3 biological replicates).

(B, C) MLFs were stimulated with 5 μg/ml cGAMP for 6 h w/ or w/o 5-10 (B) or 10 (C) μM DCPIB. The expression of *Ifnb* and *Cxcl10* was measured by RT-PCR (B) or ELISA (C) (n=3 biological replicates).

(D) MLFs were treated with cGAMP (5 μg/ml) for 1 h w or w/o 10 μM DCPIB. The cytosolic cGAMP was quantified by LC-MS (n=3 biological replicates).

(E) MLFs were treated with 5 μg/ml cGAMP for 6 h in the presence of 50 μM cisplatin (CPT) or 20 μM DCPIB. The expression of *Ifnb* and *Cxcl10* was measured by RT-PCR (n=3 biological replicates).

(F) BMDMs were stimulated with 5 μg/ml cGAMP in the presence of 50 μM CPT or 300 μM GTPγS for 6 h. The expression of *Ifnb* and *Cxcl10* was measured by RT-PCR (n=3 biological replicates).

(G) MLFs under isotonic or hypotonic conditions were stimulated with 5 μg/ml cGAMP for 3 h. The induction of *Ifnb* and *Cxcl10* was analyzed by RT-PCR (n=3 biological replicates).

(H) pMs under isotonic or hypotonic conditions were stimulated with cGAMP (1 or 5 μg/ml) for 3 h. The induction of IFN response was measured by RT-PCR (n=3 biological replicates).

Data are presented as mean ± SEM and analyzed by Student's *t* test (*p<0.05, **p<0.01, ***p<0.001). UT: untreated; n.d.: not detected.

See also Figure S4.

Figure 5. Hypotonic Swelling Enhances VRAC Transport of cGAMP and CDNs.

(A) L929 cells were stimulated with 5μg/ml cGAMP for 3 h under isotonic or hypotonic conditions. The induction of *Ifnb* and *Cxcl10* was analyzed by RT-PCR (n=3 biological replicates).

(B) L929 cells stimulated with 5 μg/ml cGAMP for 3 h under isotonic or hypotonic conditions were then cultured with normal media for another 12 h. The secretion of CXCL-10 was measured by ELISA (n=3 biological replicates).

(C) BMDMs in isotonic or hypotonic buffer were stimulated with 5 μg/ml cGAMP for 3 h. The induction of *Ifnb* and *Cxcl10* was analyzed by RT-PCR (n=3 biological replicates).

(D) MEFs were stimulated with 5 μg/ml cGAMP under isotonic or hypotonic conditions in the presence of various inhibitors (10-20 μM DCPIB; 2-10 μM CaCCinh-A01; 10-40 μM glibenclamide). The induction of *Ifnb* expression was quantified by RT-PCR (n=3 biological replicates).

(E) MEFs were pretreated with low chloride isotonic buffer for 12 h, and then stimulated with 5 μg/ml cGAMP in low chloride isotonic or hypotonic buffer. The expression of *Ifnb* was quantified by RT-PCR (n=3 biological replicates).

(F) MEFs were stimulated with 5 μg/ml cGAMP for 3 h under isotonic or hypotonic conditions. The signaling events were examined by immunoblotting. Data are representative of three independent experiments.

(G) MEFs were stimulated with 5 μg/ml 3'3'cGAMP, 10 μg/ml cdA or cdG for 3 h under hypotonic condition. The induction of *Ifnb* was analyzed by RT-PCR (n=3 biological replicates).

(H) MEFs were treated with 5 μg/ml cGAMP for 1 h under isotonic or hypotonic condition, and the cytosolic cGAMP was quantified by LC-MS (n=3 biological replicates).

(I) MEFs were treated with 5 μg/ml cGAMP for 1 h under hypotonic condition w or w/o 10 μM DCPIB. The cytosolic cGAMP was quantified by LC-MS (n=3 biological replicates).

Data are presented as mean ± SEM (* $p<0.05$, ** $p<0.01$, ***$p<0.001$; by Student's *t* test). UT: untreated; n.d.: not detected.

See also Figure S5.

Figure 6. LRRC8 VRACs Directly Transport cGAMP to Bystander Cells.

(A, B) MEFs were infected with HSV-1 (MOI: 1-5 for (A), and 5 for (B)) for 3 h. The cytosolic cGAMP was quantified by LC-MS (A), and the extracellular cGAMP was quantified by ELISA (B) (n=3 biological replicates).

(C) The supernatants from MEFs uninfected or infected with HSV-1 (MOI: 5) for 3 h were then incubated with uninfected recipient WT, *Lrrc8a*$^{-/-}$, *Sting*$^{-/-}$, or *Cgas*$^{-/-}$ MEFs for another 3 h. The induction of *Ifnβ* in the recipient MEFs was analyzed by RT-PCR (n=3 biological replicates).

(D) WT and *Lrrc8a*$^{-/-}$ MEFs were infected with adenovirus-GFP (MOI: 0.01) or MCMV-GFP (MOI: 0.01) for 24 h, and the GFP-positive cells were visualized by a

fluorescence confocal microscope and quantified by Image J (n=4 biological replicates).

(E) WT and *Lrrc8a*$^{-/-}$ MEFs transfected with STING-Cherry expressing plasmids for 12 h were then infected with adenovirus-GFP (MOI: 0.01) for another 12 h (n=4 biological replicates). White arrows indicate STING aggregates in the uninfected cells, and yellow arrows indicate STING aggregates in the infected cells.

(F) *Sting*$^{-/-}$ MEFs seeded on transwell chambers were infected with HSV-1 (MOI: 5) for 3 h, and then co-cultured with WT or *Lrrc8a*$^{-/-}$ MEFs plated on 6-well plates for 6 h. The induction of *Ifnβ* and *Mx2* in the recipient cells was analyzed by RT-PCR (n=3 biological replicates).

(G) Transwell seeded *Sting*$^{-/-}$ MEF cells and HEK293 cells were transfected with dsDNA for 3 h or a plasmid expressing cGAS for 12 h, respectively, then co-cultured with various genotypes of recipient MEFs for 9 h. The induction of *Ifnβ* in the recipient cells was analyzed by RT-PCR (n=3 biological replicates).

(H) Hypotonicity (HYPO)-activated whole-cell currents from WT and *LRRC8A*$^{-/-}$ HeLa cells with Cl^- based (50 mM NaCl) or $cGAMP^{2-}$ based (50 mM Na_2cGAMP) intracellular pipette solution. Arrows indicate the reversal potentials.

(I) Quantification of the reversal potentials of WT HeLa cells, n=9 cells for Cl^- based recording, n=6 cells for $cGAMP^{2-}$ based recording.

(J) Time-course of HYPO-activated whole-cell currents at −100 mV for WT and *LRRC8A*$^{-/-}$ HeLa cells with $cGAMP^{2-}$ based pipette solution.

(K) Quantification of baseline subtracted HYPO-activated current densities at −100 mV in WT and *LRRC8A*$^{-/-}$ HeLa cells with $cGAMP^{2-}$ based pipette solution. n=6 for each group.

Data are presented as mean ± SEM and analyzed by Student's t tests, *p<0.05, ** p<0.01, *** p<0.001. UT: untreated; UI: uninfected.

See also Figure S6.

Figure 7. LRRC8A/E-containing VRACs Promote Host Defense to HSV-1.

8-week-old WT and *Lrrc8e*$^{-/-}$ C57BL/6N littermates including both sexes were

intravenously infected with HSV-1 (1×10^7 pfu/mouse).

(A-C) The sera and tissues were collected in 24 h for ELISA (A) (n=10 mice) or RT-PCR (B, C) (n=7 mice), respectively.

(D) Plaque assay on tissues from HSV-1-infected mice for 24 h (n=4 mice).

(E) Weight loss of HSV-1-infected mice recorded daily (n=10 mice for each genotype).

Data analyzed by Student's *t* test (A-D) or two-tailed T test (E) are shown as mean ± SEM, and *p<0.05, **p<0.01, ***p<0.001. UI: uninfected.

See also Figure S7.

STAR☆METHODS

RESOURCE AVAILABILITY

Lead Contact

Further information and requests for resources and reagents should be directed to and will be fulfilled by the Lead Contact, Hui Xiao (huixiao@ips.ac.cn).

Material Availability

There is no restriction to the availability of reagents/materials generated in this study.

Data and Code Availability

Original/source data for figures in the paper is available [Mendeley Data DOI: 10.17632/ss37r6d45n.1].

EXPERIMENTAL MODEL AND SUBJECT DETAILS

Mice

All Lrrc8 VRAC-deficient mice were on C57BL/6N background, and both male and female littermates were used for all the experiments. *Lrrc8a*/*Swell1*$^{f/f}$ mice (on C57BL6 background) were generated and described previously (Yang et al., 2019). Briefly, mouse embryonic stem (ES) cells bearing a floxed *Lrrc8a* allele from the European Conditional Mouse Mutagenesis Program (EUCOMM) were used to generate chimeric mice by blastocyst injection. *Lrrc8a*$^{f/f}$ mice were bred onto Rosa26-creERT2 (B6/129) mouse strain (from Jackson Labs) to generate *Lrrc8a*$^{f/f:creERT}$ mouse in this study. *Lrrc8e*$^{-/-}$ mice were generated at the Leibniz-Forschungsinstitut für Molekulare Pharmakologie (FMP), Berlin. *Lrrc8b*$^{-/-}$, *Lrrc8c*$^{-/-}$, *Lrrc8d*$^{-/-}$ and *Lrrc8e*$^{-/-}$ (STY-051) mice were generated by Biocytogen in Beijing, China using the sgRNAs listed in Table S1. The *Sting*$^{-/-}$ and *Cgas*$^{-/-}$ mice on C57B/6J background were from the Jackson Labs. All the mice were bred and maintained in a pathogen-free animal facility at Institut Pasteur of

Shanghai. All procedures were conducted in compliance with a protocol approved by the Institutional Animal Care and Use Committee at Institut Pasteur of Shanghai.

Peritoneal Macrophages

Peritoneal macrophages were isolated from 6- to 8-weeks-old C57BL/6J mice. 3 days after intraperitoneal injection of 2 ml of 3% thioglycollate medium (BD, Cat#: 211716), peritoneal macrophages were isolated and cultured in RPMI 1640 medium supplemented with 10% FBS (HyClone, Cat#: SH30084.03), 100 U/ml penicillin, and 100 mg/ml streptomycin for use.

Bone Marrow-derived Macrophages (BMDMs)

Lrrc8a$^{f/f}$ and *Lrrc8a*$^{f/f:creERT}$ mice (6 weeks of age, sex-matched littermates on C57B6/129 background) were administered tamoxifen (Sigma-Aldrich, Cat#: T5648). 2 mg of tamoxifen in 0.2 ml corn oil was delivered by intraperitoneal injection once every two days, and 3 times in total to induce the deletion of *Lrrc8a*. Primary BMDMs and MLFs were prepared 1 week after the last injection of tamoxifen.

BMDMs were differentiated according to the method described previously (Deng et al., 2015). Bone marrow cells from 8-10 weeks old WT and *Lrrc8e*$^{-/-}$ littermates were cultured in RPMI-1640 medium supplemented with 30% L929 conditioned medium and 10% FBS for 5-7 days before use.

Mouse Lung Fibroblasts (MLFs)

MLFs were prepared from *Lrrc8a*$^{f/f}$ and *Lrrc8a*$^{f/f:creERT}$ mice injected with 3 doses of tamoxifen as described above or from 8-10 weeks old WT and *Lrrc8b*$^{-/-}$, *Lrrc8c*$^{-/-}$, *Lrrc8d*$^{-/-}$ or *Lrrc8e*$^{-/-}$ littermates using a protocol described previously (Huaux et al., 2003; Kono et al., 2007). Briefly, mouse lungs were cut into small pieces and digested with 0.1% collagenase D and trypsin in serum-free DMEM at 37°C for 1 h. Digested fibroblasts were centrifuged, washed, and then cultured in DMEM containing 10% FBS.

In 6-12 h, the nonadherent cells were washed off, and the adherent cells were cultured with DMEM containing 20% FBS, 100 U/ml penicillin and 100 mg/ml streptomycin for 5-10 days.

Mouse Embryonic Fibroblasts (MEFs)

MEFs were isolated as previously described (Lai et al., 2006). E14.5 embryos were digested overnight with 2 to 3 ml of ice-cold 0.25% trypsin-EDTA at 4°C. After vigorously pipetting, digested cells were dispersed and then spun down. After wash with PBS, embryonic cells were cultured in 10-cm dishes with DMEM containing 20% FBS, 100 U/ml penicillin and 100 mg/ml streptomycin for 5-7 days. When *Lrrc8a*$^{f/f}$ MEF cells reached approximately 70 to 90% confluence, retroviral vectors pCDH or pCDH-Cre were transducted. Following puromycin-selection for 5 days, both WT and *Lrrc8a*$^{-/-}$ MEFs were obtained for experiments.

Cell Culture

Mouse fibroblasts L929, MEFs, HeLa and human HEK293T and HEK293 (from American Type Culture Collection) were cultured in DMEM (HyClone, Cat#: SH30243.01) supplemented with 10% FBS, 100 U/ml penicillin, and 100 mg/ml streptomycin. Human THP-1 cells (from American Type Culture Collection) were cultured in RPMI 1640 medium (HyClone, Cat#: SH30809.01) supplemented with 10% FBS, 2 mM L-Glutamine, 50 μM 2-mercaptoethanol, 1 mM pyruvic acid, 100 U/ml penicillin, and 100 mg/ml streptomycin. All cell lines were checked monthly for mycoplasma contamination by commercial PCR (Lonza Mycoalert Cat#: LT07-418).

METHOD DETAILS

LC-MS/MS Quantification of cGAMP

Cellular cGAMP preparation was performed following previous protocols (Gao et al., 2015; Wu et al., 2013). Briefly, HSV-1-infected or cGAMP-incubated cells were lysed in 1 ml of lysis buffer containing 80% of methanol and 2% of acetic acid pre-chilled to

80°C. After incubation for 5 min on ice, the lysates were centrifuged at 10,000 g for 10 min, and the pellets were extracted with 0.5 ml of 2% acetic acid. The extracted cGAMP was enriched by Hyper Sep Aminopropyl SPE Columns (Thermo Scientific), and eluted with 1 ml of 4% ammonium hydroxide in 80% methanol. Following vacuum dry, the cGAMP was reconstituted in 40 μl of 50% acetonitrile and were ultrasonicated for 15 min at room temperature. After centrifugation at 14,000 rpm for 15 min, the supernatant was collected for LC-MS/MS analysis. The LC-MS/MS analysis was performed on an Agilent 1290 UPLC (Agilent, USA) coupled to an AB Sciex 6500 Triple Quad mass spectrometer (AB Sciex, USA) with the electrospray ionization (ESI) source. A Waters ACQUITY UPLC BEH Amide column (1.7 μm, 2.1×100 mm) was used for GAMP separation with a flow rate at 0.4 ml/min and column temperature of 45°C. The mobile phases were comprised of (A) 0.2% formic acid and 10 mM Ammonium acetate in 50% acetonitrile and (B) 0.2% formic acid and 10 mM ammonium acetate in 95% acetonitrile. The gradient elution was 80% B kept for 1.0 min, then changed linearly to 5% B during 7.0 min, increased to 80% B in 7.1 min and maintained for 2.9 min. The injection volume was set to 2 μL. The mass parameters were as follows: ion spray voltage was 5500 V, ion source temperature was 500°C, collision gas was Medium, ion source gas 1 was 50 psi, ion source gas 2 was 60 psi, curtain gas was 35 psi. Multiple Reaction Monitoring (MRM) was used to monitor GAMP in the positive ion mode. The proposed assay exhibits a good linear range of 2.5–500 ng/mL (2.5, 5, 10, 25, 50, 100, 250 and 500 ng/mL) for GAMP, which sufficiently covers the typical levels determined in actual samples.

Quantification of cGAMP by ELISA or Functional Assay

MEFs of various genotypes (5×10^4 cells in total) were seeded on a 48-well plate and infected with HSV-1 (MOI: 5) for 3 h. The supernatant was collected and cGAMP was measured by Cayman Chemical 2’3’-cGAMP ELISA Kit (Interchim, Cat#:501700) according to manufacturer’s instruction.

For extracellular cGAMP functional assay, 1×10^7 MEF cells were infected with HSV-1 (MOI: 5) for 3 h, and cell media were collected and centrifuged at 13,000 rpm for 10 min. After discarding insoluble pellets, the supernatants were digested with 1000 U/ml of Benzonase at 37°C for 40 min in the presence or absence of 0.5U/ml of snake venom PDE (Sigma, isolated from Crotalus adamanteus) (Ablasser et al., 2013b; Bridgeman et al., 2015). Afterwards the supernatants were heated at 95°C for 10 min, followed by centrifugation at 13,000 rpm for 10 min, and then added to recipient MEFs of various genotypes for 3 h prior to RNA extraction and real-time PCR analysis of IFN response.

ELISA Assay

BMDMs, MEFs, and MLFs were infected with various MOIs of HSV-1 or VSV for 16-24 h, or treated with 5-10 μg/ml of 2'3'cGAMP for 12 h. The amounts of IFN-β, CXCL-10, CCL-5 and TNF were assessed with ELISA kits according to the manufacturers' recommendations (CCL-5 ELISA, peprotech Cat#: 900-K124; IP-10 ELISA, peprotech Cat#: 900-K153; IFN-β ELISA, Biolegend Cat#: 439407 and TNF ELISA, Systems from eBioscience.

Hypotonicity-induced Cell Swelling

Cells were incubated with isotonic buffer (110 mM mannitol, 90 mM NaCl, 2 mM KCl, 1mM $MgCl_2$, 1 mM $CaCl_2$, and 10 mM HEPES, pH 7.4), hypotonic buffer (10 mM mannitol, 90 mM NaCl, 2 mM KCl, 1mM $MgCl_2$, 1 mM $CaCl_2$, and 10 mM HEPES, pH 7.4) or hypertonic buffer (220 mM mannitol, 90 mM NaCl, 2 mM KCl, 1mM $MgCl_2$, 1 mM $CaCl_2$, and 10 mM HEPES, pH 7.4) for 3 h, in the absence or presence of cGAMP.

For chloride-depletion, 90 mM sodium chloride in both isotonic and hypotonic buffer was replaced with 90 mM sodium gluconate.

Transwell Assay

The upper cells, such as HEK293 cells (2.5×10^5 per ml) transiently transfected with either empty vector or cGAS-expressing plasmid (4μg/ml) for 12 h, WT or *Sting*$^{-/-}$ MEFs transfected with dsDNA (8 μg/ml, lipofectamine) for 3 h, or WT or *Sting*$^{-/-}$ MEFs infected with HSV-1 (MOI: 5) for 3 h, were grown on a transwell (6-well Transwell with 0.4 μm pores from Corning, Cat# 3450) before co-culture with the recipient bystander cells. After transfection or infection, the culture media were removed, and the upper cells were washed 2-3 times with PBS prior to co-culture with the recipient cells. The recipient cells, including MEFs and MLFs of various genotypes (2×10^5 per ml), were pre-seeded on 6-well culture plates, and grew separately until co-culture with various upper cells in the transwell chamber for another 6 h. In the case of DCPIB treatment, DCPIB (20 μM) was added into the recipient cells 30 min before co-culture, and presented throughout the entire course of co-culture. Subsequently, the transwell chamber was removed and the recipient cells were collected for RNA preparation and RT-PCR analysis for IFN response.

siRNA Design and Transfection

siRNAs targeting *Lrrc8a-e*, *Cx43*, or *Panx1* were ordered from GenePharma and listed in Table S1. SiRNAs were transfected to cells by Lipofectamine RNAiMAX Transfection Reagent (Thermo Fisher Cat#: 13778030) for 2-3 days before stimulation.

Gene Targeting with CRISPR-Cas9 in L929 Cells

SgRNAs against *Lrrc8a or Lrrc8e* were designed (https://www.genscript.com/gRNA-design-tool.html) and listed in Table S1. The annealed sgRNA oligos were cloned into pLentiCRISPR plasmid (Addgene #78852), and packaged in HEK 293T cells. Viral media were harvested after 50 h. The Lenti-viruses-containing media were passed through a 0.45 μm filter and added to L929 cells under selection with 1.5 mg/mL puromycin (Sigma Aldrich) for 1 week. and puromycin-resistant clones were screened followed by DNA sequencing.

RNA Preparation and Real-Time (RT)-PCR

Total RNAs were extracted from L929, MEF and THP1 and peritoneal macrophages using TRIzol (Invitrogen, Cat#: 10296010) according to the manufacturer's instruction. cDNA was reversely transcribed from 500 ng total RNA by PrimeScript RT-PCR kit (Takara, Cat#: RR014). RT-PCR was carried out with primer pairs listed in Table S1 on an ABI 7900HT Fast RT-PCR System. Data shown were the relative abundance of the indicated mRNA normalized to that of *Gapdh* by the change-in-cycling-threshold (ΔΔCT) method.

Viral Infection and Plaque Assay

MEFs, L929 cells and MLFs (5×10^5 per ml) were infected with HSV-1 or VSV in serum-free medium for 2 h as described previously (Ma et al., 2017). Afterwards, virus-containing medium was removed and replaced with serum-containing DMEM medium. In 12 h post-infection, cells were harvested and RNAs were prepared by TRIzol. To check viral-induced cell death, 1.5 h after viral-infected, the supernatant was removed and cells were overlaid by 2×MEM containing 1.6% agar. 36 h post infection stained with 0.5% crystal violet dissolved in 4% formaldehyde for 2 h. Viral titers (pfu/ml) were calculated based on counted plaques.

8-weeks old sex-matched littermates on C57BL/6N background were intravenously injected with HSV-1 (KOS strain, 1×10^7 plaque-forming units PFU) and VSV (Indiana strain, 5×10^6 pfu) in 0.1 ml PBS (Ma et al., 2017), and the weight-loss of the infected mice was monitored daily up to 10 days. In 24 h post-infection, mouse sera were collected for ELISA, and the organs such as kidney, liver and spleen were removed and homogenized for RNA preparation and real-time PCR analyses.

HSV-1 and VSV plaque assay was performed as described previously (Du et al., 2015; Ma et al., 2017). Briefly, the supernatants harvested from virus-infected cells were serial diluted in serum-free DMEM and then added into confluent Vero cells cultured

on 6-well plates. In 1 h, supernatants were removed and cells were overlaid by 4% methylcellulose. Three days later, the overlay medium was removed and cells were fixed with 4% formaldehyde for 1 h and then stained with 0.5% crystal violet. Viral titers (pfu/ml) were calculated based on counted plaques.

Confocal Fluorescence Microscopy

MEFs were transfected with pLVX-N-mCherry-hSTING by Lipofectamine 2000 Transfection Reagent (Thermo Fisher, Cat#: 11668019) for 12 h. Subsequently, the liposomal/DNA-containing media were removed and transfected cells were infected with Adeno-virus-GFP (MOI: 0.01) or MCMV BAC *pSMgfp* (MOI: 0.01) for 24 h (Adeno-virus-GFP (Li et al., 2015) was kindly provided by Hongbin Ji from Institute of Biochemistry and Cell Biology, Shanghai, China; and MCMV BAC *pSMgfp* (Pan et al., 2018) was kindly provided by Zhikang Qian from Institut Pasteur of Shanghai, China). Next, the virus infected cells or cGAMP-treated cells were fixed with 4% paraformaldehyde for 10 min and stained with DAPI for 5 min at room temperature. The fluorescence images were collected on a laser capture confocal microscope (FV1200, Olympus) using separate laser excitation to avoid any cross-interference between different fluorophores.

Electrophysiology

Whole-cell patch-clamp recordings were performed as described previously (Yang et al., 2019). HeLa cells were plated onto coverslips 24-48 h before recording. For hypotonicity-activated VRAC current recordings, HeLa or HCT116 cells were whole-cell patched in isotonic bath solution containing (in mM): 50 NaCl, 10 HEPES, 200 mannitol (pH adjusted to pH 7.3 with NaOH and osmolality adjusted to 310 mOsm/kg), then hypotonic solution (HYPO) contains the same ionic composition but with only 100 mannitol were applied. Recording pipettes were pulled by a micropipette puller (P-1000, Sutter instrument) and had a resistance of 5-10 MΩ when filled with the Cl^- based intracellular solution containing (in mM): 50 NaCl, 10 HEPES, 200 mannitol (pH

adjusted to pH 7.3 with NaOH and osmolality adjusted to 310 mOsm/kg). $cGAMP^{2-}$ based intracellular solution was made by replacing 50 NaCl and 200 mannitol with 50 Na_2cGAMP (from ChemieTek) and 150 mannitol to maintain the same osmolality. Relative permeability of $cGAMP^{2-}$ to Cl^- was estimated based on the reversal potential difference as described previously (Caldwell et al., 1986). The voltage ramp protocol (5 s or 15 s interval, 500 ms or 2.5 s duration) was used with a holding potential of 0 mV and depolarized from −100 to +100 mV. Recordings were made with MultiClamp 700B amplifier and 1550B digitizer (Molecular Device) or an EPC-10 amplifier. Data acquisition were performed with pClamp 10.7 (Molecular Device) or Patchmatser (HEKA) software, filtered at 1 kHz and digitized at 10 kHz.

QUANTIFICATION AND STATISTICAL ANALYSIS

All data are shown as mean values, and error bars represent SEM from the number of assays indicated (from at least three independent experiments). For statistical comparisons, data were analyzed by an unpaired two-tailed Student's t test (*$p<0.05$, **$p<0.01$, ***$p<0.001$; by Student's t test) to determine differences between groups using Prism software (GraphPad Software).

REFERENCES

Ablasser, A., and Chen, Z.J. (2019). cGAS in action: Expanding roles in immunity and inflammation. Science *363*.

Ablasser, A., Goldeck, M., Cavlar, T., Deimling, T., Witte, G., Rohl, I., Hopfner, K.P., Ludwig, J., and Hornung, V. (2013a). cGAS produces a 2'-5'-linked cyclic dinucleotide second messenger that activates STING. Nature *498*, 380-384.

Ablasser, A., and Hur, S. (2020). Regulation of cGAS- and RLR-mediated immunity to nucleic acids. Nat Immunol *21*, 17-29.

Ablasser, A., Schmid-Burgk, J.L., Hemmerling, I., Horvath, G.L., Schmidt, T., Latz, E., and Hornung, V. (2013b). Cell intrinsic immunity spreads to bystander cells via the intercellular transfer of cGAMP. Nature *503*, 530-534.

Barber, G.N. (2015). STING: infection, inflammation and cancer. Nat Rev Immunol *15*, 760-770.

Benfenati, V., Caprini, M., Nicchia, G.P., Rossi, A., Dovizio, M., Cervetto, C., Nobile, M., and Ferroni, S. (2009). Carbenoxolone inhibits volume-regulated anion conductance in cultured rat cortical astroglia. Channels (Austin) *3*, 323-336.

Best, L., Brown, P.D., Sener, A., and Malaisse, W.J. (2010). Electrical activity in pancreatic islet cells: The VRAC hypothesis. Islets *2*, 59-64.

Bridgeman, A., Maelfait, J., Davenne, T., Partridge, T., Peng, Y., Mayer, A., Dong, T., Kaever, V., Borrow, P., and Rehwinkel, J. (2015). Viruses transfer the antiviral second messenger cGAMP between cells. Science *349*, 1228-1232.

Caldwell, J.H., Van Brunt, J., and Harold, F.M. (1986). Calcium-dependent anion channel in the water mold, Blastocladiella emersonii. The Journal of membrane biology *89*, 85-97.

Chen, Q., Boire, A., Jin, X., Valiente, M., Er, E.E., Lopez-Soto, A., Jacob, L., Patwa, R., Shah, H., Xu, K.*, et al.* (2016a). Carcinoma-astrocyte gap junctions promote brain metastasis by cGAMP transfer. Nature *533*, 493-498.

Chen, Q., Sun, L., and Chen, Z.J. (2016b). Regulation and function of the cGAS-STING pathway of cytosolic DNA sensing. Nat Immunol *17*, 1142-1149.

Christensen, M.H., Jensen, S.B., Miettinen, J.J., Luecke, S., Prabakaran, T., Reinert, L.S., Mettenleiter, T., Chen, Z.J., Knipe, D.M., Sandri-Goldin, R.M.*, et al.* (2016). HSV-1 ICP27 targets the TBK1-activated STING signalsome to inhibit virus-induced type I IFN expression. EMBO J *35*, 1385-1399.

Danilchanka, O., and Mekalanos, J.J. (2013). Cyclic dinucleotides and the innate immune response. Cell *154*, 962-970.

Decher, N., Lang, H.J., Nilius, B., Bruggemann, A., Busch, A.E., and Steinmeyer, K. (2001). DCPIB is a novel selective blocker of I(Cl,swell) and prevents swelling-induced shortening of guinea-pig atrial action potential duration. Br J Pharmacol *134*, 1467-1479.

Deng, Z., Ma, S., Zhou, H., Zang, A., Fang, Y., Li, T., Shi, H., Liu, M., Du, M., Taylor, P.R.*, et al.* (2015). Tyrosine phosphatase SHP-2 mediates C-type lectin receptor-induced activation of the kinase Syk and anti-fungal TH17 responses. Nat Immunol *16*, 642-652.

Du, M., Liu, J., Chen, X., Xie, Y., Yuan, C., Xiang, Y., Sun, B., Lan, K., Chen, M., James, S.J.*, et al.* (2015). Casein kinase II controls TBK1/IRF3 activation in IFN response against viral infection. J Immunol *194*, 4477-4488.

Friard, J., Tauc, M., Cougnon, M., Compan, V., Duranton, C., and Rubera, I. (2017). Comparative Effects of Chloride Channel Inhibitors on LRRC8/VRAC-Mediated Chloride Conductance. Frontiers in pharmacology *8*, 328.
Gao, D., Li, T., Li, X.D., Chen, X., Li, Q.Z., Wight-Carter, M., and Chen, Z.J. (2015). Activation of cyclic GMP-AMP synthase by self-DNA causes autoimmune diseases. Proc Natl Acad Sci U S A *112*, E5699-5705.
Gentili, M., Kowal, J., Tkach, M., Satoh, T., Lahaye, X., Conrad, C., Boyron, M., Lombard, B., Durand, S., Kroemer, G.*, et al.* (2015). Transmission of innate immune signaling by packaging of cGAMP in viral particles. Science *349*, 1232-1236.
Gentili, M., Lahaye, X., Nadalin, F., Nader, G.P.F., Lombardi, E.P., Herve, S., De Silva, N.S., Rookhuizen, D.C., Zueva, E., Goudot, C.*, et al.* (2019). The N-Terminal Domain of cGAS Determines Preferential Association with Centromeric DNA and Innate Immune Activation in the Nucleus. Cell reports *26*, 3798.
Gradogna, A., Gavazzo, P., Boccaccio, A., and Pusch, M. (2017). Subunit-dependent oxidative stress sensitivity of LRRC8 volume-regulated anion channels. J Physiol *595*, 6719-6733.
Hoffmann, E.K., Lambert, I.H., and Pedersen, S.F. (2009). Physiology of cell volume regulation in vertebrates. Physiol Rev *89*, 193-277.
Holmgren, A.M., McConkey, C.A., and Shin, S. (2017). Outrunning the Red Queen: bystander activation as a means of outpacing innate immune subversion by intracellular pathogens. Cell Mol Immunol *14*, 14-21.
Huaux, F., Liu, T., McGarry, B., Ullenbruch, M., and Phan, S.H. (2003). Dual roles of IL-4 in lung injury and fibrosis. J Immunol *170*, 2083-2092.
Ishikawa, H., and Barber, G.N. (2008). STING is an endoplasmic reticulum adaptor that facilitates innate immune signalling. Nature *455*, 674-678.
Ishikawa, H., Ma, Z., and Barber, G.N. (2009). STING regulates intracellular DNA-mediated, type I interferon-dependent innate immunity. Nature *461*, 788-792.
Jentsch, T.J. (2016). VRACs and other ion channels and transporters in the regulation of cell volume and beyond. Nat Rev Mol Cell Biol *17*, 293-307.
Kang, C., Xie, L., Gunasekar, S.K., Mishra, A., Zhang, Y., Pai, S., Gao, Y., Kumar, A., Norris, A.W., Stephens, S.B., and Sah, R. (2018). SWELL1 is a glucose sensor regulating beta-cell excitability and systemic glycaemia. Nat Commun *9*, 367.
Kono, Y., Nishiuma, T., Nishimura, Y., Kotani, Y., Okada, T., Nakamura, S., and Yokoyama, M. (2007). Sphingosine kinase 1 regulates differentiation of human and mouse lung fibroblasts mediated by TGF-beta1. American journal of respiratory cell and molecular biology *37*, 395-404.
Kumar, L., Chou, J., Yee, C.S., Borzutzky, A., Vollmann, E.H., von Andrian, U.H., Park, S.Y., Hollander, G., Manis, J.P., Poliani, P.L., and Geha, R.S. (2014). Leucine-rich repeat containing 8A (LRRC8A) is essential for T lymphocyte development and function. J Exp Med *211*, 929-942.
Lai, W.S., Parker, J.S., Grissom, S.F., Stumpo, D.J., and Blackshear, P.J. (2006). Novel mRNA targets for tristetraprolin (TTP) identified by global analysis of stabilized transcripts in TTP-deficient fibroblasts. Molecular and cellular biology *26*, 9196-9208.
Lam, E., Stein, S., and Falck-Pedersen, E. (2014). Adenovirus detection by the cGAS/STING/TBK1 DNA sensing cascade. J Virol *88*, 974-981.

Lee, C.C., Freinkman, E., Sabatini, D.M., and Ploegh, H.L. (2014). The protein synthesis inhibitor blasticidin s enters mammalian cells via leucine-rich repeat-containing protein 8D. J Biol Chem *289*, 17124-17131.
Li, F., Han, X., Li, F., Wang, R., Wang, H., Gao, Y., Wang, X., Fang, Z., Zhang, W., Yao, S*., et al.* (2015). LKB1 Inactivation Elicits a Redox Imbalance to Modulate Non-small Cell Lung Cancer Plasticity and Therapeutic Response. Cancer cell *27*, 698-711.
Liu, H., Moura-Alves, P., Pei, G., Mollenkopf, H.J., Hurwitz, R., Wu, X., Wang, F., Liu, S., Ma, M., Fei, Y*., et al.* (2019). cGAS facilitates sensing of extracellular cyclic dinucleotides to activate innate immunity. EMBO reports *20*.
Luck, J.C., Puchkov, D., Ullrich, F., and Jentsch, T.J. (2018). LRRC8/VRAC anion channels are required for late stages of spermatid development in mice. J Biol Chem *293*, 11796-11808.
Luo, W.W., Li, S., Li, C., Lian, H., Yang, Q., Zhong, B., and Shu, H.B. (2016). iRhom2 is essential for innate immunity to DNA viruses by mediating trafficking and stability of the adaptor STING. Nat Immunol *17*, 1057-1066.
Luteijn, R.D., Zaver, S.A., Gowen, B.G., Wyman, S.K., Garelis, N.E., Onia, L., McWhirter, S.M., Katibah, G.E., Corn, J.E., Woodward, J.J., and Raulet, D.H. (2019). SLC19A1 transports immunoreactive cyclic dinucleotides. Nature *573*, 434-438.
Lutter, D., Ullrich, F., Lueck, J.C., Kempa, S., and Jentsch, T.J. (2017). Selective transport of neurotransmitters and modulators by distinct volume-regulated LRRC8 anion channels. J Cell Sci *130*, 1122-1133.
Ma, S., Wan, X., Deng, Z., Shi, L., Hao, C., Zhou, Z., Zhou, C., Fang, Y., Liu, J., Yang, J*., et al.* (2017). Epigenetic regulator CXXC5 recruits DNA demethylase Tet2 to regulate TLR7/9-elicited IFN response in pDCs. J Exp Med *214*, 1471-1491.
Marcus, A., Mao, A.J., Lensink-Vasan, M., Wang, L., Vance, R.E., and Raulet, D.H. (2018). Tumor-Derived cGAMP Triggers a STING-Mediated Interferon Response in Non-tumor Cells to Activate the NK Cell Response. Immunity *49*, 754-763 e754.
Margolis, S.R., Wilson, S.C., and Vance, R.E. (2017). Evolutionary Origins of cGAS-STING Signaling. Trends Immunol.
Nilius, B., Voets, T., Prenen, J., Barth, H., Aktories, K., Kaibuchi, K., Droogmans, G., and Eggermont, J. (1999). Role of Rho and Rho kinase in the activation of volume-regulated anion channels in bovine endothelial cells. J Physiol *516 (Pt 1)*, 67-74.
Osei-Owusu, J., Yang, J., Vitery, M.D.C., and Qiu, Z. (2018). Molecular Biology and Physiology of Volume-Regulated Anion Channel (VRAC). Current topics in membranes *81*, 177-203.
Pan, D., Han, T., Tang, S., Xu, W., Bao, Q., Sun, Y., Xuan, B., and Qian, Z. (2018). Murine Cytomegalovirus Protein pM91 Interacts with pM79 and Is Critical for Viral Late Gene Expression. J Virol *92*.
Pedersen, S.F., Okada, Y., and Nilius, B. (2016). Biophysics and Physiology of the Volume-Regulated Anion Channel (VRAC)/Volume-Sensitive Outwardly Rectifying Anion Channel (VSOR). Pflugers Arch *468*, 371-383.
Planells-Cases, R., Lutter, D., Guyader, C., Gerhards, N.M., Ullrich, F., Elger, D.A., Kucukosmanoglu, A., Xu, G., Voss, F.K., Reincke, S.M*., et al.* (2015). Subunit composition of VRAC channels determines substrate specificity and cellular resistance to Pt-based anti-cancer drugs. EMBO J *34*, 2993-3008.

Platt, C.D., Chou, J., Houlihan, P., Badran, Y.R., Kumar, L., Bainter, W., Poliani, P.L., Perez, C.J., Dent, S.Y., Clapham, D.E.*, et al.* (2017). Leucine-rich repeat containing 8A (LRRC8A)-dependent volume-regulated anion channel activity is dispensable for T-cell development and function. J Allergy Clin Immunol.
Qiu, Z., Dubin, A.E., Mathur, J., Tu, B., Reddy, K., Miraglia, L.J., Reinhardt, J., Orth, A.P., and Patapoutian, A. (2014). SWELL1, a plasma membrane protein, is an essential component of volume-regulated anion channel. Cell *157*, 447-458.
Ritchie, C., Cordova, A.F., Hess, G.T., Bassik, M.C., and Li, L. (2019). SLC19A1 Is an Importer of the Immunotransmitter cGAMP. Molecular cell.
Roers, A., Hiller, B., and Hornung, V. (2016). Recognition of Endogenous Nucleic Acids by the Innate Immune System. Immunity *44*, 739-754.
Schober, A.L., Wilson, C.S., and Mongin, A.A. (2017). Molecular composition and heterogeneity of the LRRC8-containing swelling-activated osmolyte channels in primary rat astrocytes. J Physiol *595*, 6939-6951.
Stempel, M., Chan, B., Juranic Lisnic, V., Krmpotic, A., Hartung, J., Paludan, S.R., Fullbrunn, N., Lemmermann, N.A., and Brinkmann, M.M. (2019). The herpesviral antagonist m152 reveals differential activation of STING-dependent IRF and NF-kappaB signaling and STING's dual role during MCMV infection. EMBO J *38*.
Stuhlmann, T., Planells-Cases, R., and Jentsch, T.J. (2018). LRRC8/VRAC anion channels enhance beta-cell glucose sensing and insulin secretion. Nat Commun *9*, 1974.
Su, L., Quade, B., Wang, H., Sun, L., Wang, X., and Rizo, J. (2014). A plug release mechanism for membrane permeation by MLKL. Structure *22*, 1489-1500.
Sun, L., Wu, J., Du, F., Chen, X., and Chen, Z.J. (2013). Cyclic GMP-AMP synthase is a cytosolic DNA sensor that activates the type I interferon pathway. Science *339*, 786-791.
Sun, W., Li, Y., Chen, L., Chen, H., You, F., Zhou, X., Zhou, Y., Zhai, Z., Chen, D., and Jiang, Z. (2009). ERIS, an endoplasmic reticulum IFN stimulator, activates innate immune signaling through dimerization. Proc Natl Acad Sci U S A *106*, 8653-8658.
Varela, D., Simon, F., Riveros, A., Jorgensen, F., and Stutzin, A. (2004). NAD(P)H oxidase-derived H(2)O(2) signals chloride channel activation in cell volume regulation and cell proliferation. J Biol Chem *279*, 13301-13304.
Voets, T., Manolopoulos, V., Eggermont, J., Ellory, C., Droogmans, G., and Nilius, B. (1998). Regulation of a swelling-activated chloride current in bovine endothelium by protein tyrosine phosphorylation and G proteins. J Physiol *506 (Pt 2)*, 341-352.
Voss, F.K., Ullrich, F., Munch, J., Lazarow, K., Lutter, D., Mah, N., Andrade-Navarro, M.A., von Kries, J.P., Stauber, T., and Jentsch, T.J. (2014). Identification of LRRC8 heteromers as an essential component of the volume-regulated anion channel VRAC. Science *344*, 634-638.
Wang, X., Li, Y., Liu, S., Yu, X., Li, L., Shi, C., He, W., Li, J., Xu, L., Hu, Z.*, et al.* (2014). Direct activation of RIP3/MLKL-dependent necrosis by herpes simplex virus 1 (HSV-1) protein ICP6 triggers host antiviral defense. Proc Natl Acad Sci U S A *111*, 15438-15443.
Wilson, C.S., Bach, M.D., Ashkavand, Z., Norman, K.R., Martino, N., Adam, A.P., and Mongin, A.A. (2019). Metabolic constraints of swelling-activated glutamate release in astrocytes and their implication for ischemic tissue damage. Journal of neurochemistry.

Wu, J., Sun, L., Chen, X., Du, F., Shi, H., Chen, C., and Chen, Z.J. (2013). Cyclic GMP-AMP is an endogenous second messenger in innate immune signaling by cytosolic DNA. Science *339*, 826-830.
Yang, J., Vitery, M.D.C., Chen, J., Osei-Owusu, J., Chu, J., and Qiu, Z. (2019). Glutamate-Releasing SWELL1 Channel in Astrocytes Modulates Synaptic Transmission and Promotes Brain Damage in Stroke. Neuron *102*, 813-827 e816.
Zhong, B., Yang, Y., Li, S., Wang, Y.Y., Li, Y., Diao, F., Lei, C., He, X., Zhang, L., Tien, P., and Shu, H.B. (2008). The adaptor protein MITA links virus-sensing receptors to IRF3 transcription factor activation. Immunity *29*, 538-550.
Zhou, Y., Fei, M., Zhang, G., Liang, W.C., Lin, W., Wu, Y., Piskol, R., Ridgway, J., McNamara, E., Huang, H.*, et al.* (2020). Blockade of the Phagocytic Receptor MerTK on Tumor-Associated Macrophages Enhances P2X7R-Dependent STING Activation by Tumor-Derived cGAMP. Immunity *52*, 357-373 e359.

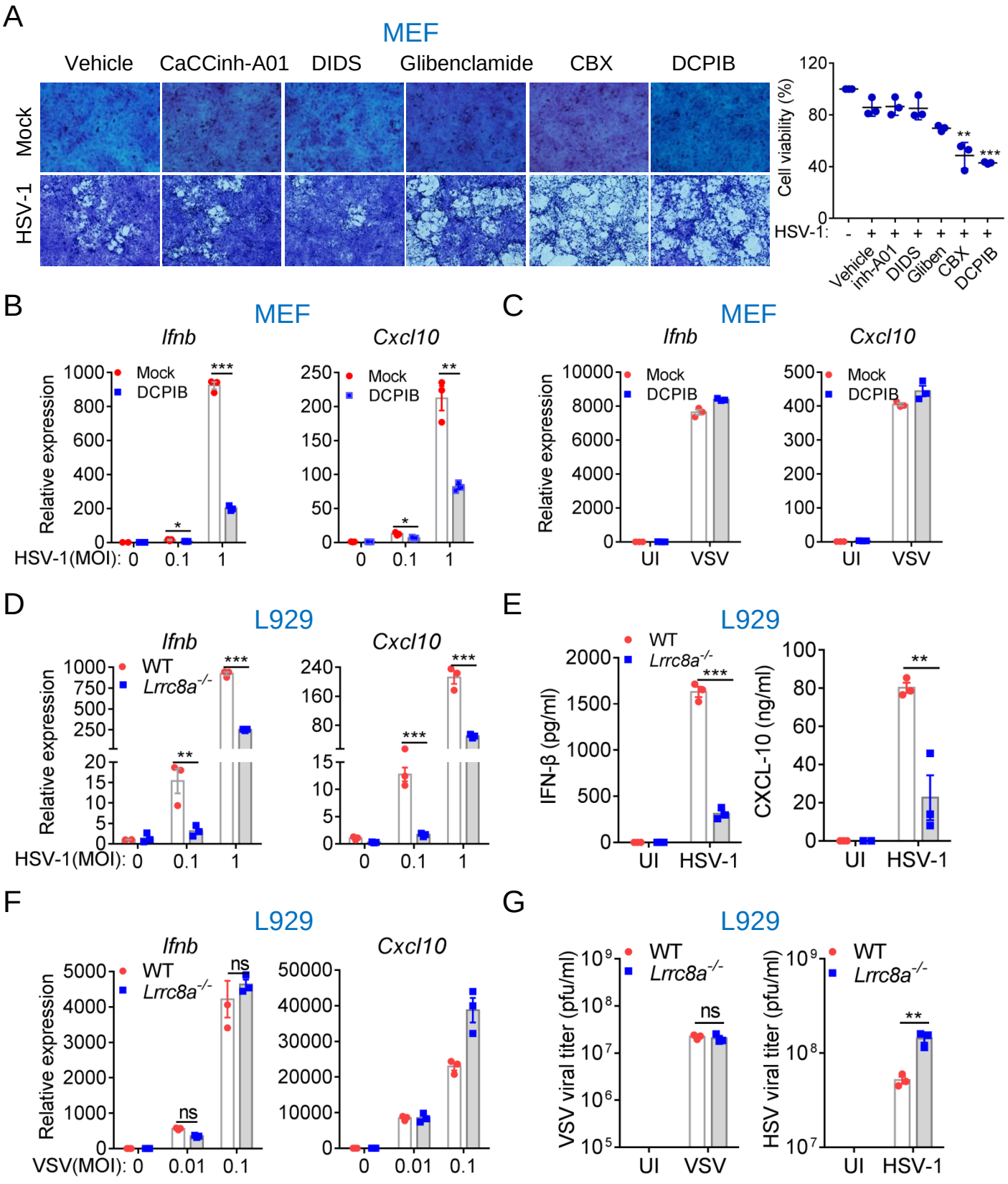
A
MEF
Vehicle
CaCCinh-A01
DIDS
Glibenclamide
CBX
DCPIB
Mock
HSV-1
Cell viability (%)
HSV-1:
Vehicle
Inh-A01
DIDS
Gliben
CBX
DCPIB
B
MEF
Ifnb
Cxcl10
Relative expression
Mock
DCPIB
HSV-1(MOI):
C
MEF
Ifnb
Cxcl10
Relative expression
Mock
DCPIB
UI
VSV
D
L929
Ifnb
Cxcl10
Relative expression
WT
Lrrc8a-/-
HSV-1(MOI):
E
L929
WT
Lrrc8a-/-
IFN-β (pg/ml)
CXCL-10 (ng/ml)
UI
HSV-1
F
L929
Ifnb
Cxcl10
Relative expression
WT
Lrrc8a-/-
ns
VSV(MOI):
G
L929
WT
Lrrc8a-/-
VSV viral titer (pfu/ml)
HSV viral titer (pfu/ml)
ns
UI
VSV
HSV-1

Figure 1

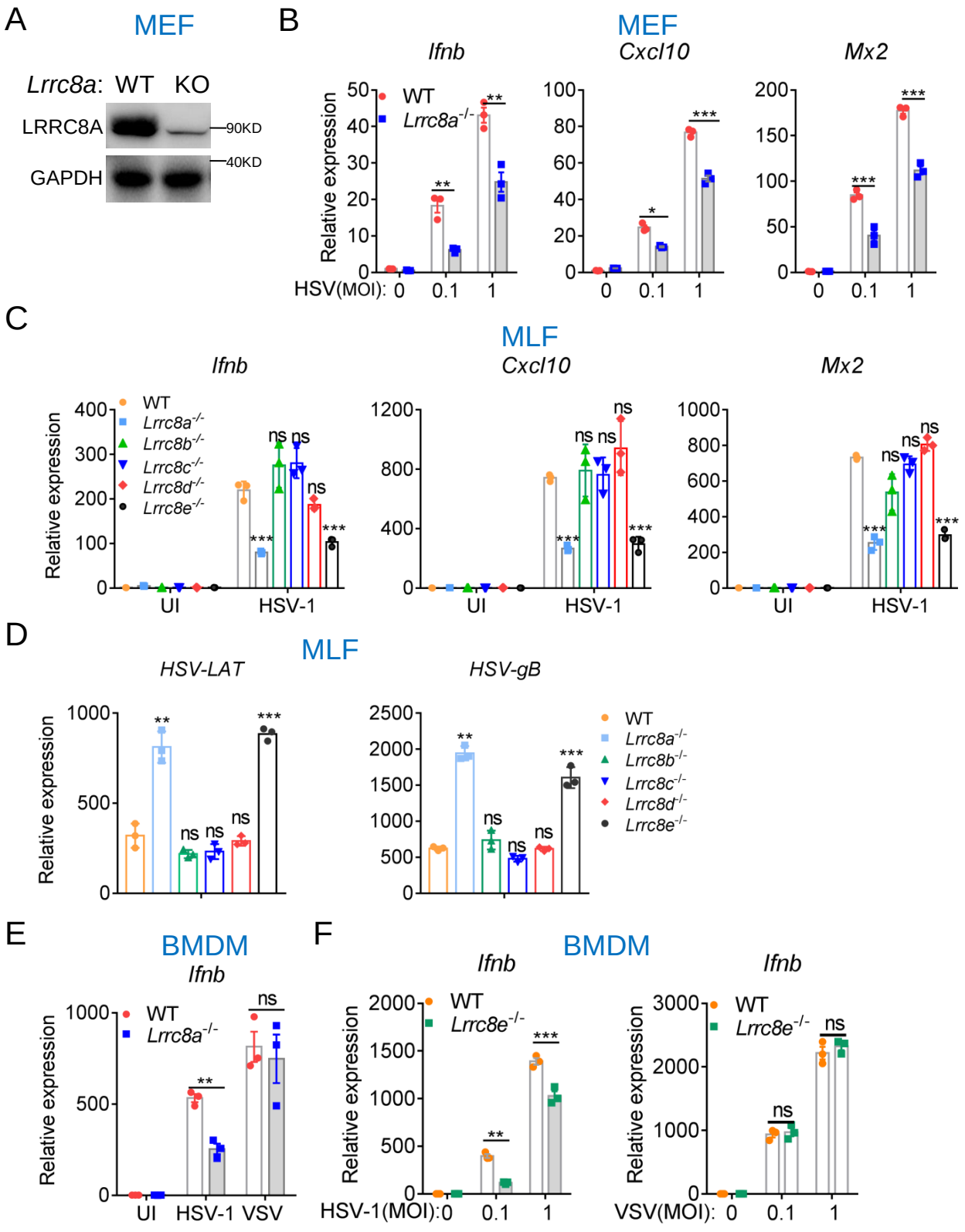
A
MEF
Lrrc8a: WT KO
LRRC8A
90KD
GAPDH
40KD
B
MEF
Ifnb
Cxcl10
Mx2
Relative expression
WT
Lrrc8a-/-
HSV(MOI): 0 0.1 1
C
MLF
Ifnb
Cxcl10
Mx2
Relative expression
WT
Lrrc8a-/-
Lrrc8b-/-
Lrrc8c-/-
Lrrc8d-/-
Lrrc8e-/-
UI
HSV-1
D
MLF
HSV-LAT
HSV-gB
Relative expression
E
BMDM
Ifnb
Relative expression
UI HSV-1 VSV
F
BMDM
Ifnb
Ifnb
Relative expression
WT
Lrrc8e-/-
HSV-1(MOI): 0 0.1 1
VSV(MOI): 0 0.1 1

Figure 2

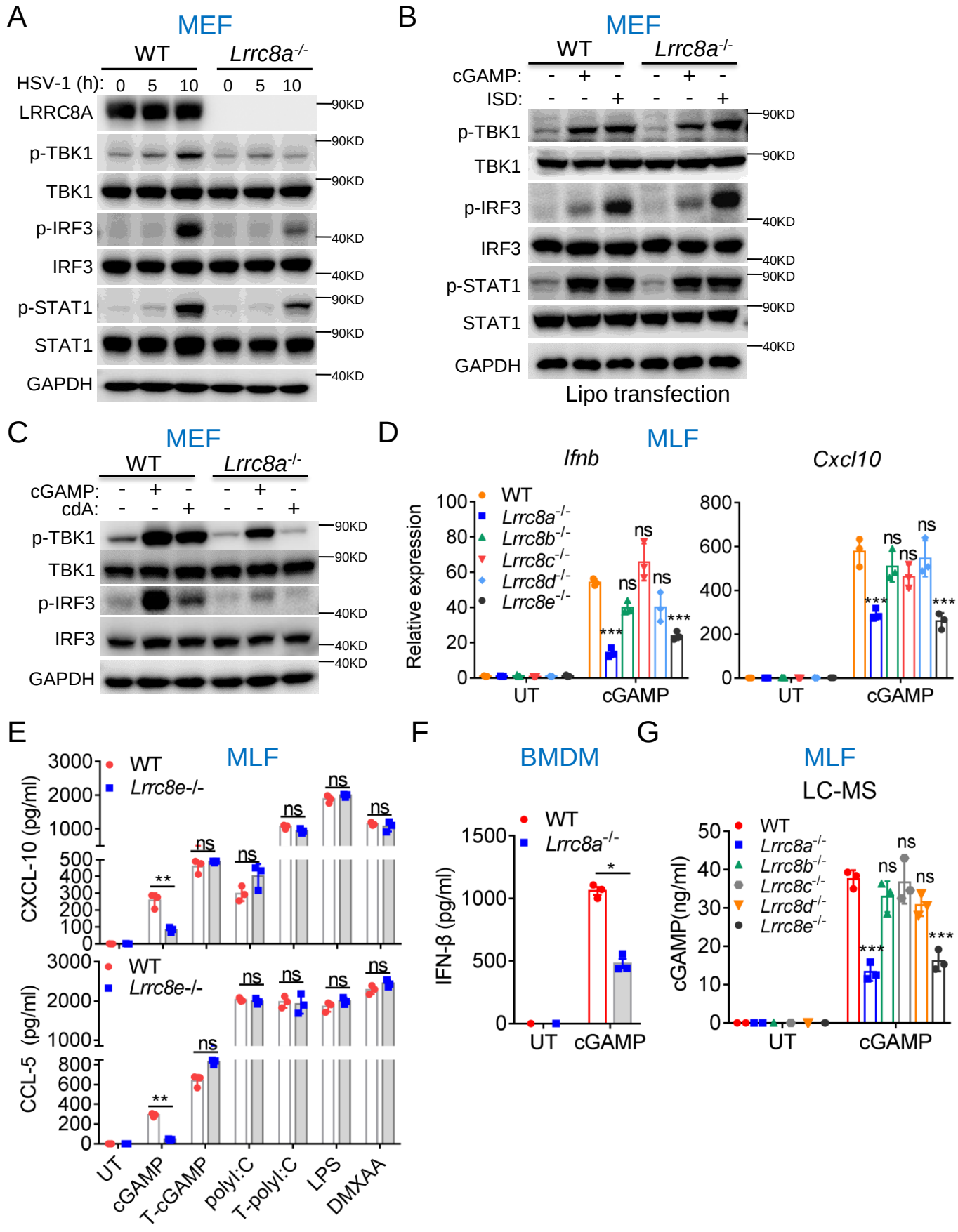
A
MEF
WT
Lrrc8a-/-
HSV-1 (h): 0 5 10 0 5 10
LRRC8A
p-TBK1
TBK1
p-IRF3
IRF3
p-STAT1
STAT1
GAPDH
90KD
40KD
B
MEF
WT
Lrrc8a-/-
cGAMP:
ISD:
Lipo transfection
C
MEF
cGAMP:
cdA:
D
MLF
Ifnb
Cxcl10
Relative expression
WT
Lrrc8a-/-
Lrrc8b-/-
Lrrc8c-/-
Lrrc8d-/-
Lrrc8e-/-
UT
cGAMP
E
MLF
CXCL-10 (pg/ml)
CCL-5 (pg/ml)
Lrrc8e-/-
T-cGAMP
polyI:C
T-polyI:C
LPS
DMXAA
F
BMDM
IFN-β (pg/ml)
G
MLF
LC-MS
cGAMP(ng/ml)

Figure 3

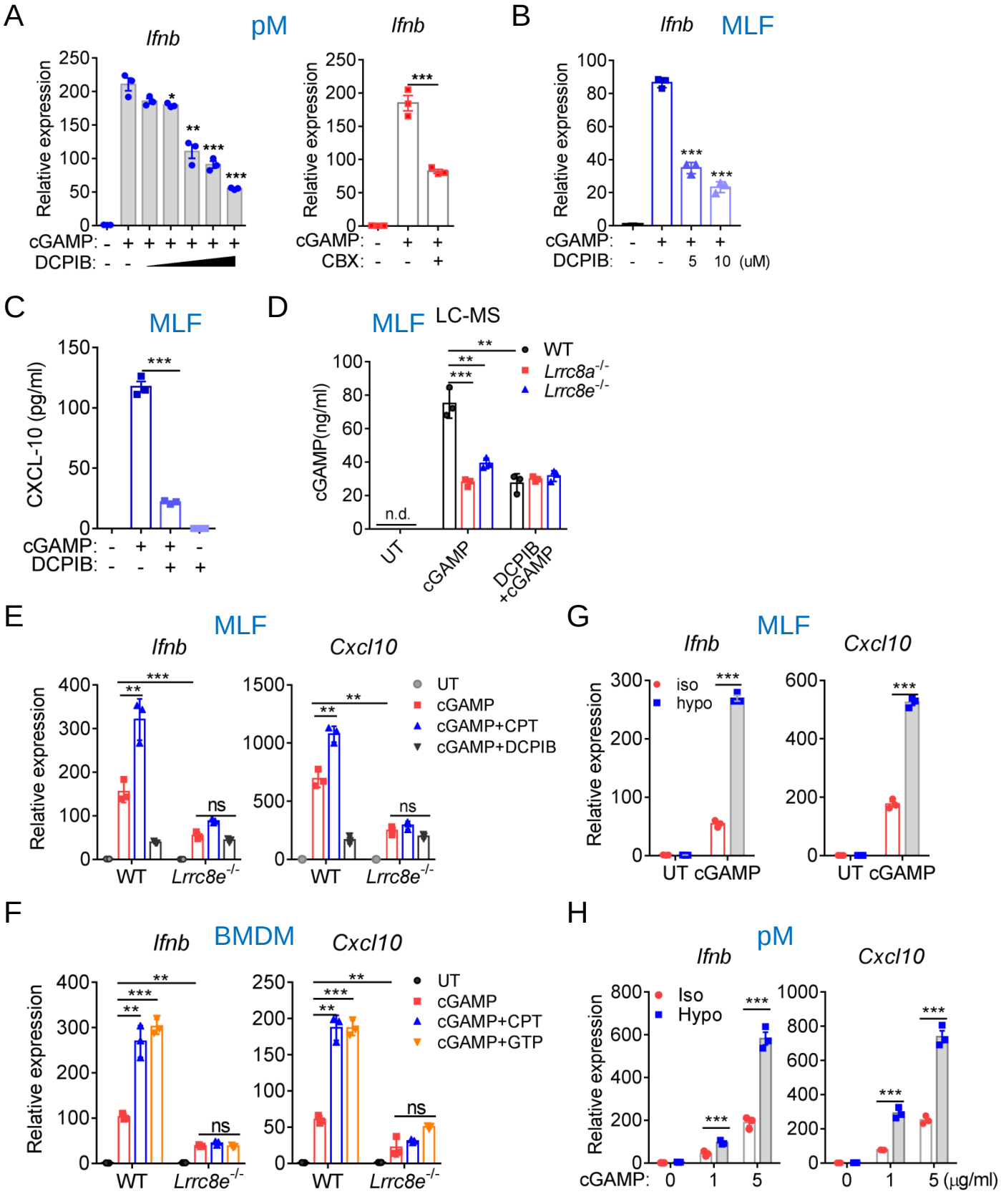
A
pM
Ifnb
Relative expression
cGAMP:
DCPIB:
Ifnb
CBX:
B
Ifnb
MLF
C
MLF
CXCL-10 (pg/ml)
D
MLF
LC-MS
cGAMP(ng/ml)
n.d.
WT
Lrrc8a-/-
Lrrc8e-/-
UT
cGAMP
DCPIB +cGAMP
E
MLF
Ifnb
Cxcl10
UT
cGAMP
cGAMP+CPT
cGAMP+DCPIB
ns
WT
Lrrc8e-/-
G
MLF
iso
hypo
F
BMDM
cGAMP+GTP
H
pM
Iso
Hypo
(μg/ml)

Figure 4

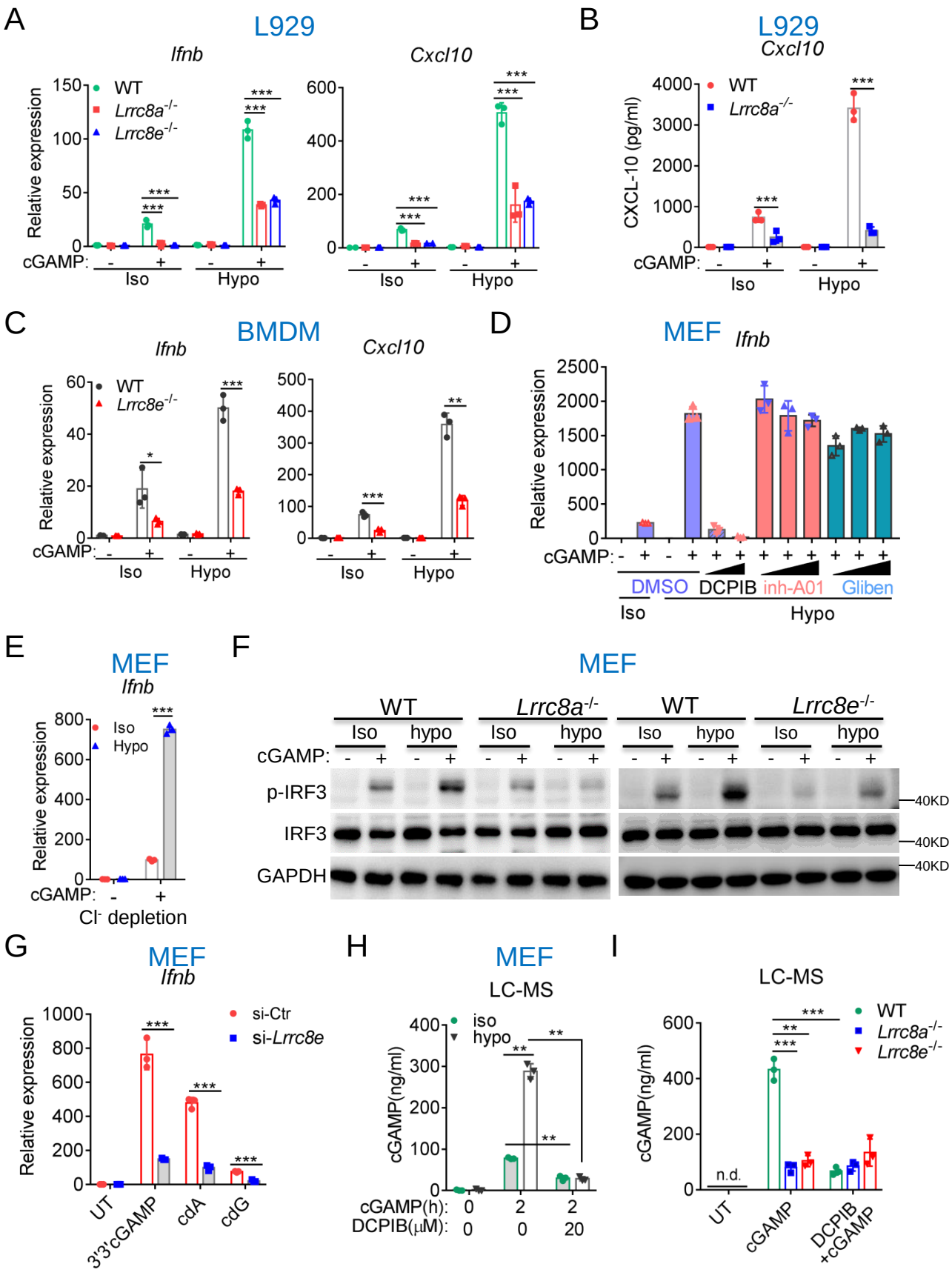
A
L929
Ifnb
Cxcl10
Relative expression
WT
Lrrc8a-/-
Lrrc8e-/-
cGAMP:
Iso
Hypo
B
L929
Cxcl10
CXCL-10 (pg/ml)
C
BMDM
Ifnb
Cxcl10
D
MEF
Ifnb
DMSO
DCPIB
inh-A01
Gliben
E
MEF
Ifnb
Cl- depletion
F
MEF
p-IRF3
IRF3
GAPDH
40KD
G
MEF
Ifnb
si-Ctr
si-Lrrc8e
UT
3'3'cGAMP
cdA
cdG
H
MEF
LC-MS
cGAMP(ng/ml)
cGAMP(h):
DCPIB(μM):
I
LC-MS
n.d.
UT
cGAMP
DCPIB +cGAMP

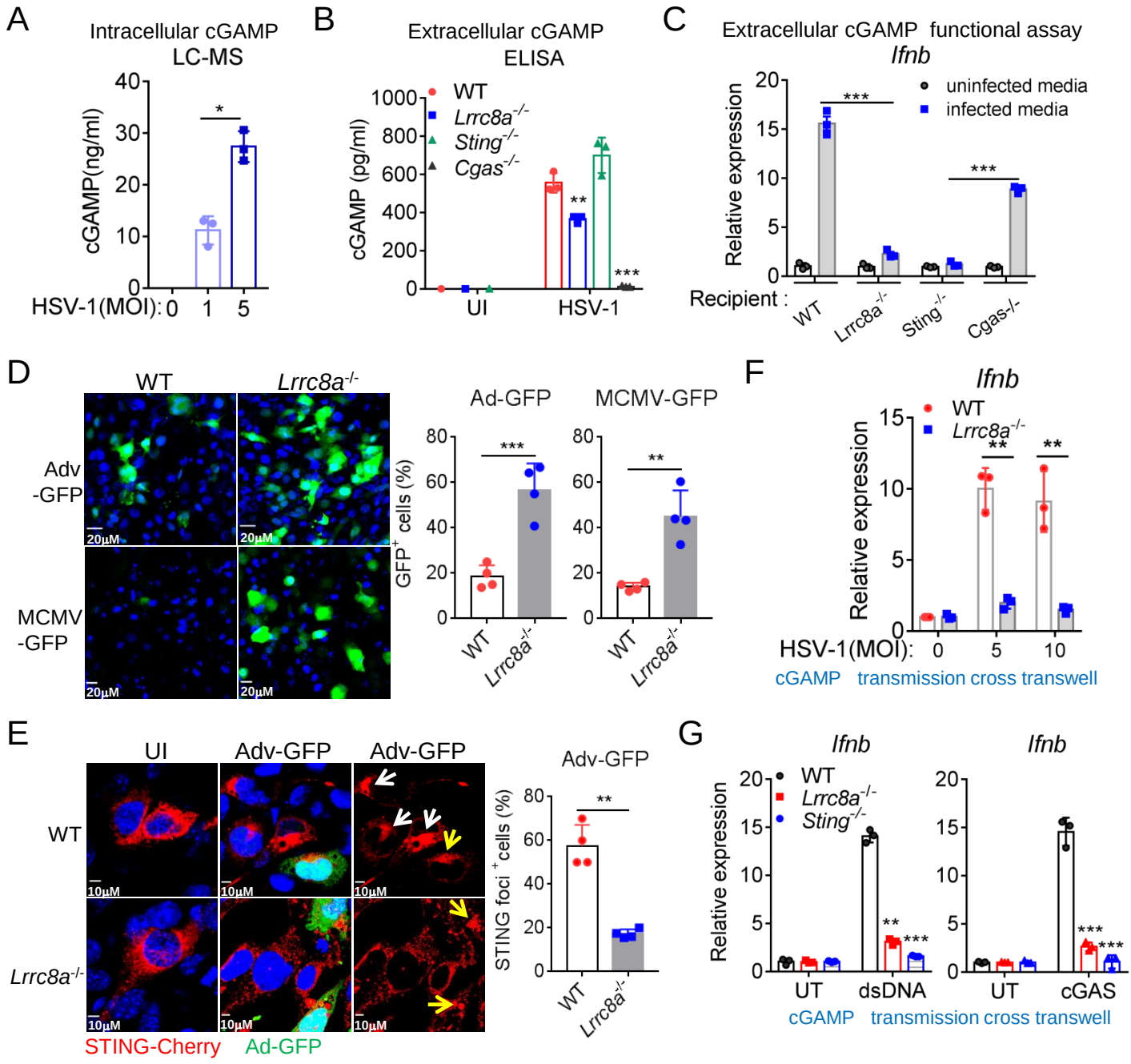
A
Intracellular cGAMP
LC-MS
cGAMP(ng/ml)
HSV-1(MOI): 0 1 5
B
Extracellular cGAMP
ELISA
cGAMP (pg/ml)
WT
Lrrc8a-/-
Sting-/-
Cgas-/-
UI
HSV-1
C
Extracellular cGAMP functional assay
Ifnb
Relative expression
uninfected media
infected media
Recipient :
WT
Lrrc8a-/-
Sting-/-
Cgas-/-
D
WT
Lrrc8a-/-
Adv -GFP
MCMV -GFP
20μM
Ad-GFP
MCMV-GFP
GFP+ cells (%)
F
Ifnb
Relative expression
HSV-1(MOI): 0 5 10
cGAMP transmission cross transwell
E
UI
Adv-GFP
Adv-GFP
WT
Lrrc8a-/-
10μM
STING foci + cells (%)
STING-Cherry
Ad-GFP
G
Ifnb
Ifnb
Sting-/-
UT
dsDNA
cGAS
cGAMP transmission cross transwell
H
I (nA)
WT [Cl-]in
WT [cGAMP2-]in
8A-/-[cGAMP2-]in
V (mV)
I
Reversal potential (mV)
[Cl-]in [cGAMP2-]in
J
HYPO WT [cGAMP2-]in
100 pA
1 min
HYPO 8A-/- [cGAMP2-]in
K
WT
8A-/-
Current density pA/pF

Figure 6

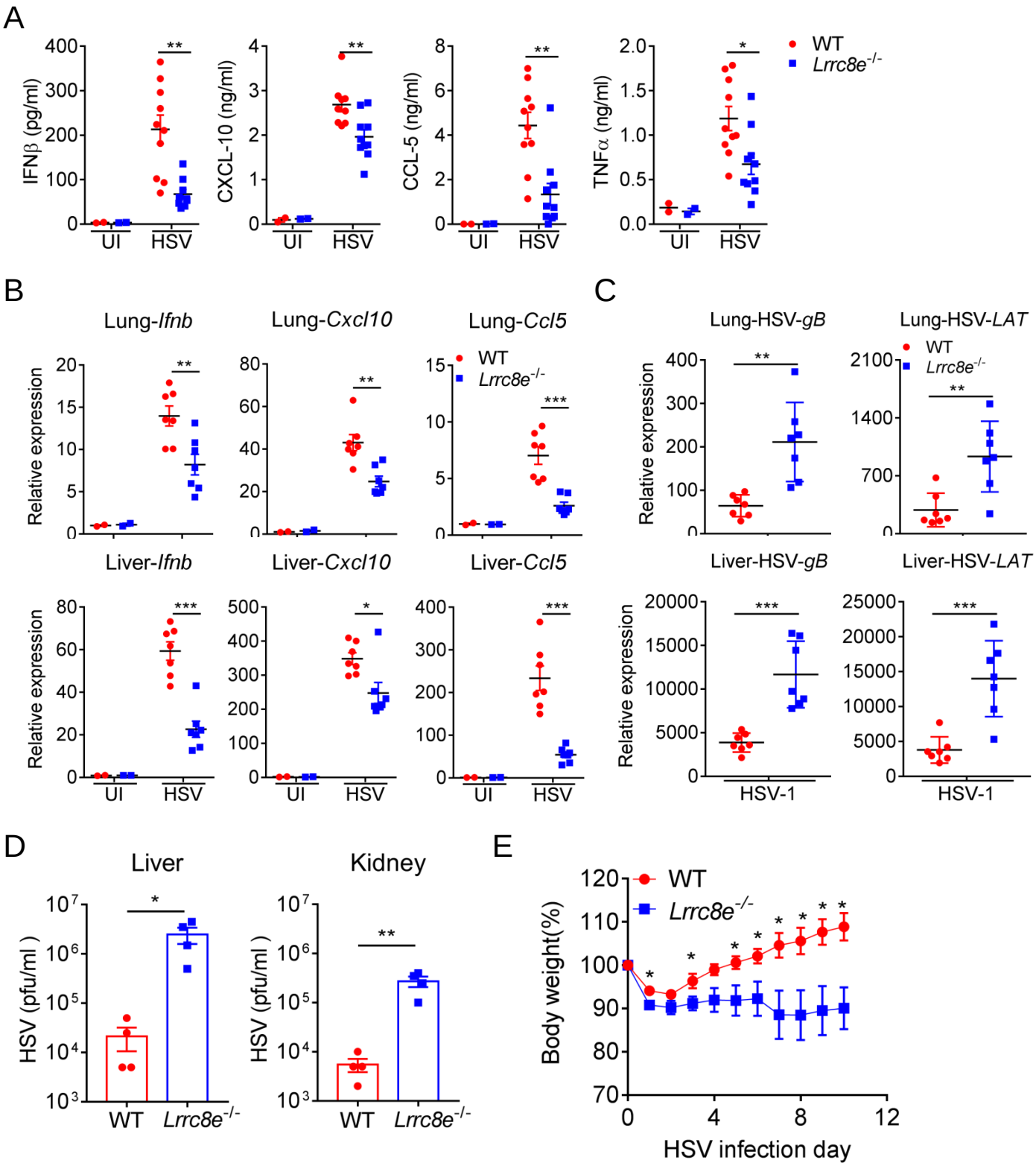
A
IFNβ (pg/ml)
CXCL-10 (ng/ml)
CCL-5 (ng/ml)
TNFα (ng/ml)
UI
HSV
WT
Lrrc8e-/-
B
Lung-Ifnb
Lung-Cxcl10
Lung-Ccl5
Liver-Ifnb
Liver-Cxcl10
Liver-Ccl5
Relative expression
C
Lung-HSV-gB
Lung-HSV-LAT
Liver-HSV-gB
Liver-HSV-LAT
HSV-1
D
Liver
Kidney
HSV (pfu/ml)
E
Body weight(%)
HSV infection day

Figure 7

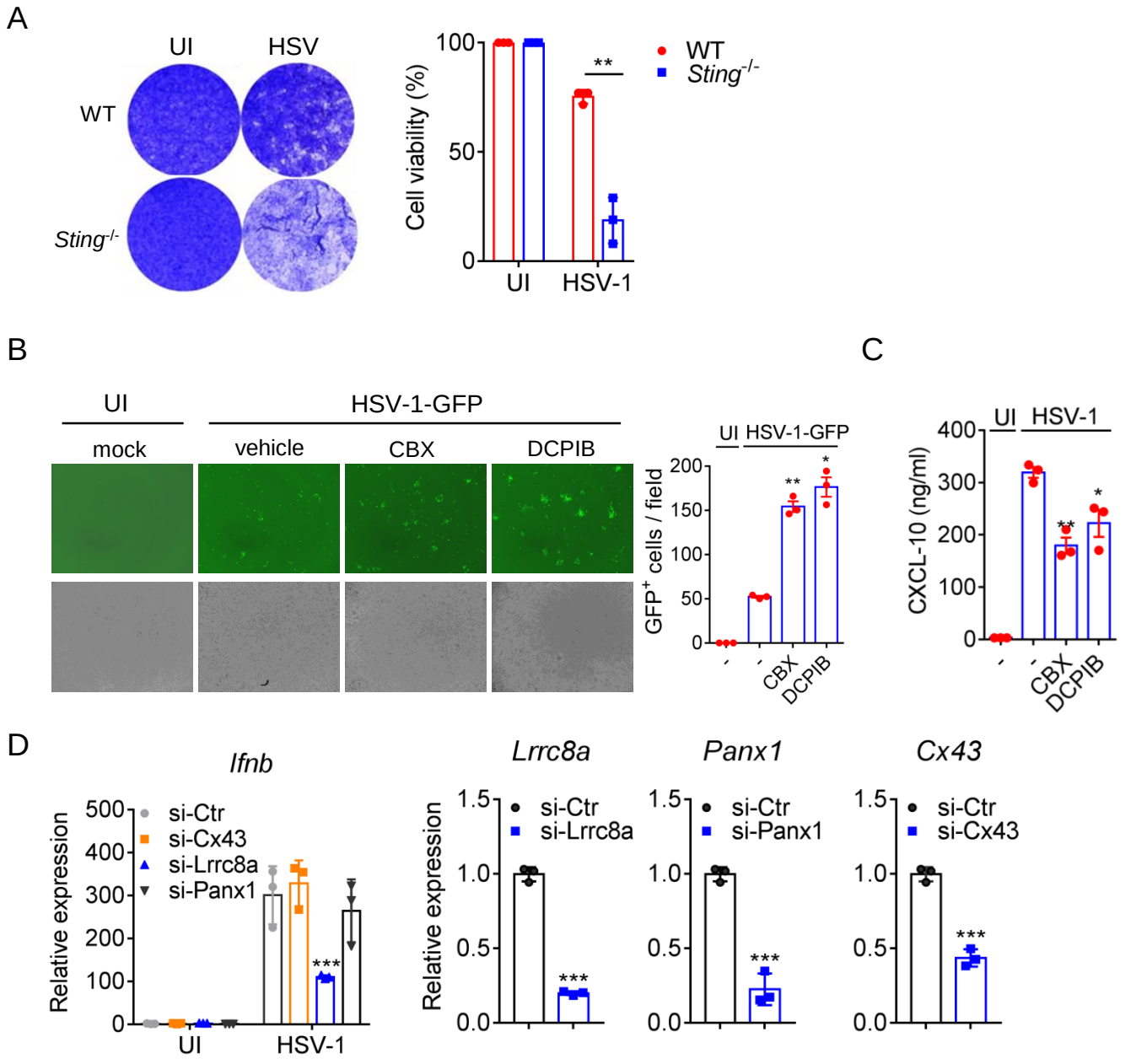

Figure S1 HSV-1-stimulated IFN-β and CXCL-10 Production Depends on VRAC, Related to Figure 1

(**A**) WT and *Sting*$^{-/-}$ MEFs were uninfected (UI) or infected with HSV-1 (MOI: 0.01) for 36 h. Infected cells were fixed and stained with 0.5% crystal violet for 2 h, and the images were collected by CTL immunospot imager. Cell viability was quantified by Image J (cells positive-stained as blue were regarded as live cells).
(**B**) L929 cells were infected with HSV-1-GFP (MOI: 0.1) with or without 100 μM CBX or 20 μM DCPIB for 36 h (n=3 biological replicates).
(**C**) L929 cells were infected with HSV-1 (MOI: 0.1) for 24 h with or without 100 μM CBX or 20 μM DCPIB. CXCL-10 production was measured by ELISA (n=3 biological replicates).
(**D**) L929 cells transfected with various siRNAs for 48 h were then infected with HSV-1 (MOI: 0.1) for 12 h. The gene expression was quantified by RT-PCR (n=3 biological replicates).
Data are presented as mean ± SEM (*p<0.05, **p<0.01, ***p<0.001; analyzed by Student's *t* test).

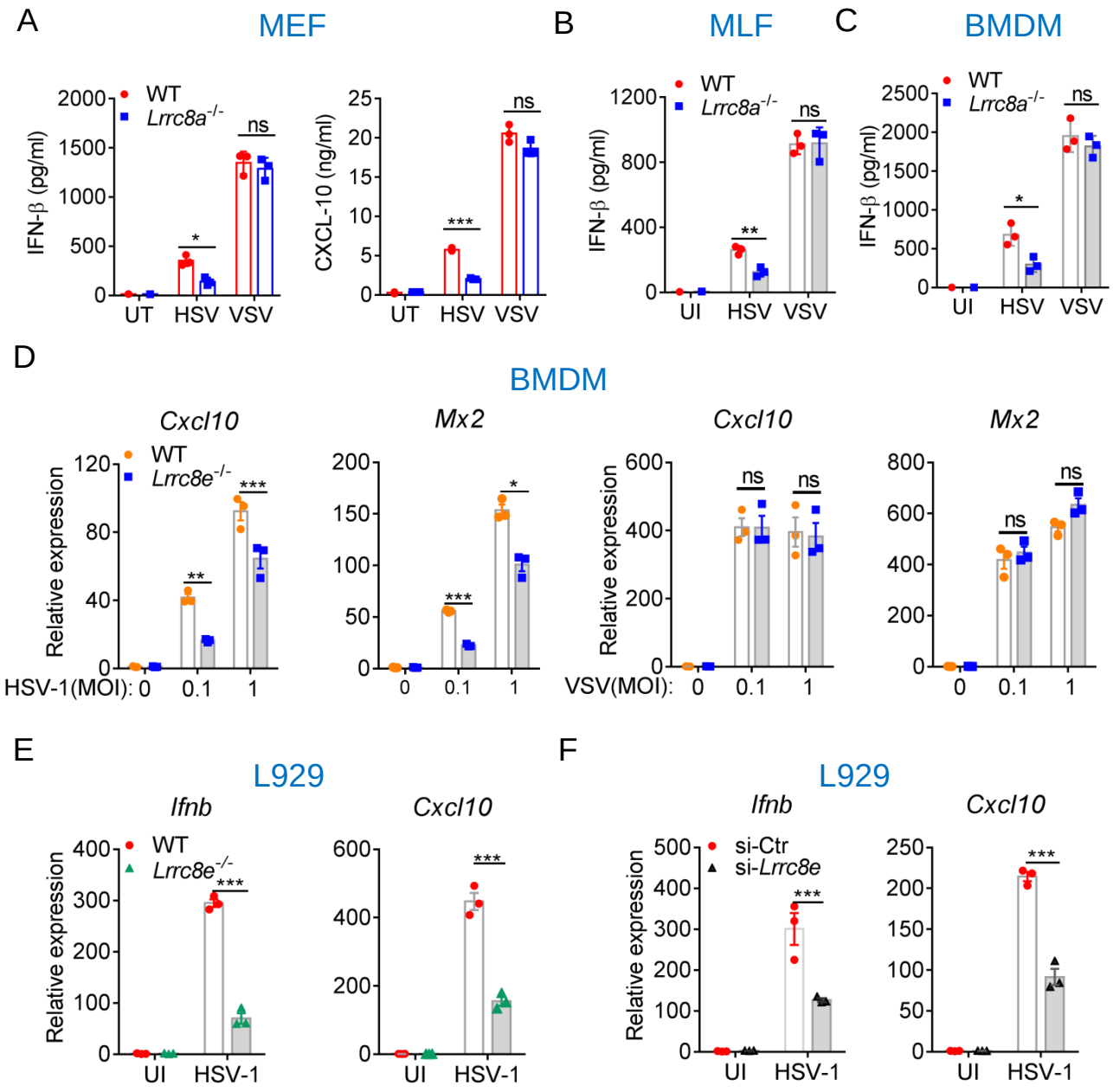

Figure S2 HSV-1-induced IFN Response Depends on Lrrc8e, Related to Figure 2

(**A-C**) MEFs, MLFs and BMDMs were infected with HSV-1 (MOI: 0.1) or VSV (0.01) for 18 h, and the secreted IFNβ was assessed by ELISA (n=3 biological replicates).
(**D**) WT and *Lrrc8e*$^{-/-}$ BMDMs were infected with HSV-1 or VSV for 9 h, and the expression of Isgs was quantified by RT-PCR (n=3 biological replicates).
(**E**) WT and *Lrrc8e*$^{-/-}$ L929 cells were infected with HSV-1 (MOI: 0.1) for 12 h. The expression of *Ifnb* and *Cxcl10* was quantified by RT-PCR (n=3 biological replicates).
(**F**) L929 cells transfected with control or *Lrrc8e* siRNAs for 48 h were infected with HSV-1 (MOI: 0.1). The expression of *Ifnb*, *Cxcl10* and *Lrrc8e* was quantified by RT-PCR (n=3 biological replicates).
Data are presented as mean ± SEM (*p<0.05, **p<0.01, ***p<0.001 and ns: not significant; analyzed by Student's *t* test). UI: uninfected.

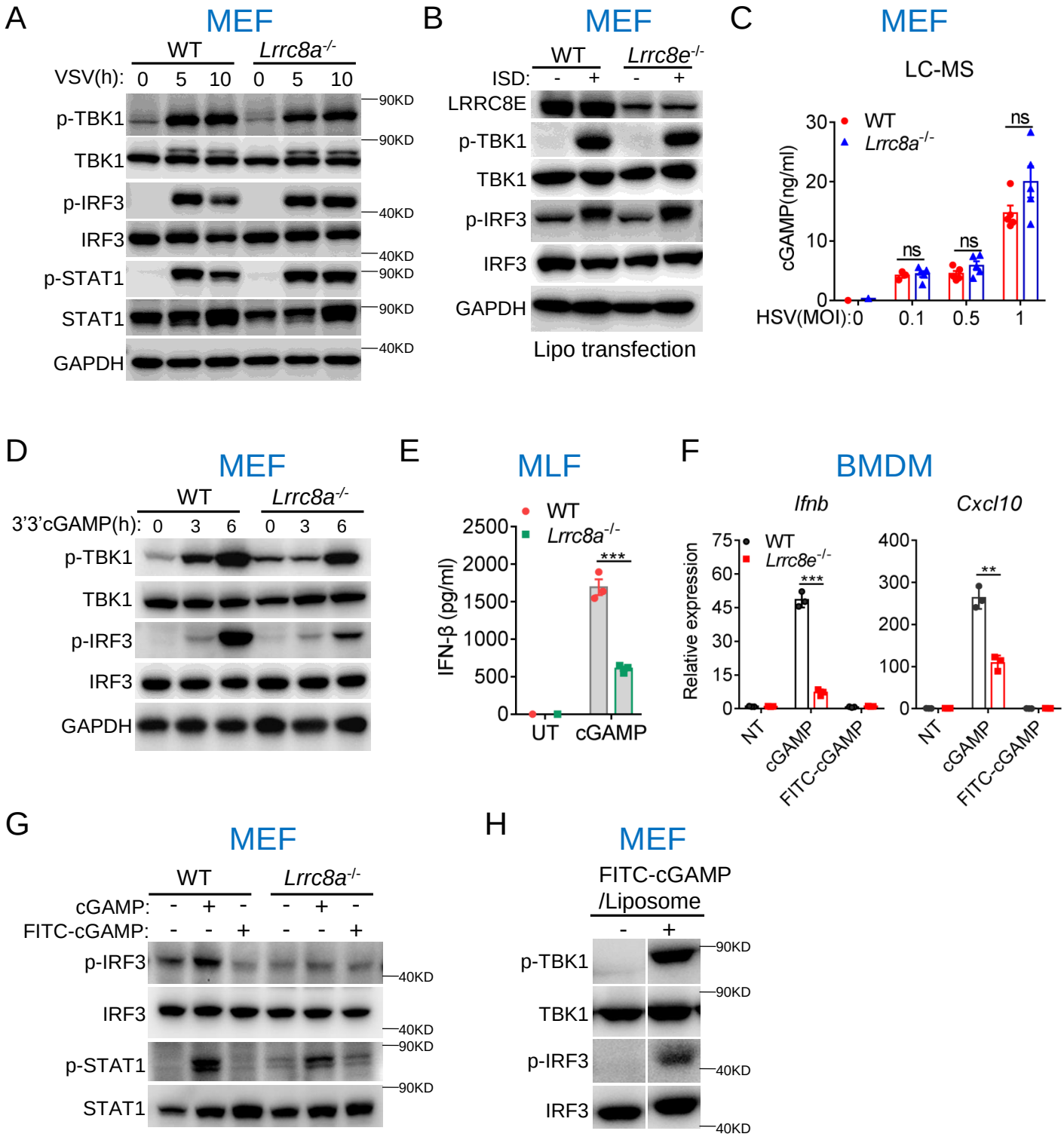

Figure S3 Response to Intracellularly Applied cGAMP or Extracellular FITC-cGAMP Does Not Depend on Lrrc8a or Lrrc8e, Related to Figure 3

(**A**) WT and *Lrrc8a*$^{-/-}$ MEFs were infected with VSV (MOI: 0.1), and the TBK1/IRF3 signaling was assessed by immunoblotting. Data are representative of three independent experiments.
(**B**) WT and *Lrrc8e*$^{-/-}$ MEFs were transfected with 1 μg/ml ISD with lipofectamine for 3 h. Immunoblotting was conducted for STING signaling. Data are representative of two independent experiments.
(**C**) The intracellular cGAMP from WT and *Lrrc8a*$^{-/-}$ MEFs infected with HSV-1 for 3 h was quantified by LC-MS (n=3 biological replicates).

(**D**) WT and *Lrrc8a*$^{-/-}$ MEFs were stimulated with 10 μg/ml 3'3'cGAMP added without transfection reagent for 2 h. Data are representative of three independent experiments.
(**E**) WT and *Lrrc8a*$^{-/-}$ MLFs were stimulated with 5 μg/ml cGAMP for 12 h, and the supernatants were collected for ELISA (n=3 biological replicates).
(**F**) WT and *Lrrc8e*$^{-/-}$ BMDMs were stimulated with 10 μg/ml cGAMP or FITC-cGAMP without transfection for 3 h. The expression of *Ifnb* and *Cxcl10* was quantified by RT-PCR (n=3 biological replicates).
(**G**) WT and *Lrrc8a*$^{-/-}$ MEFs were incubated with 10 μg/ml cGAMP or FITC-cGAMP for 3 h. Data are representative of two independent experiments.
(**H**) WT and *Lrrc8a*$^{-/-}$ MEFs were transfected with FITC-cGAMP (2 μg/ml) with Lipofectamine for 3 h. Data are presented as mean ± SEM (*$p<0.05$, **$p<0.01$, ***$p<0.001$ and ns: not significant; analyzed by Student's *t* test).

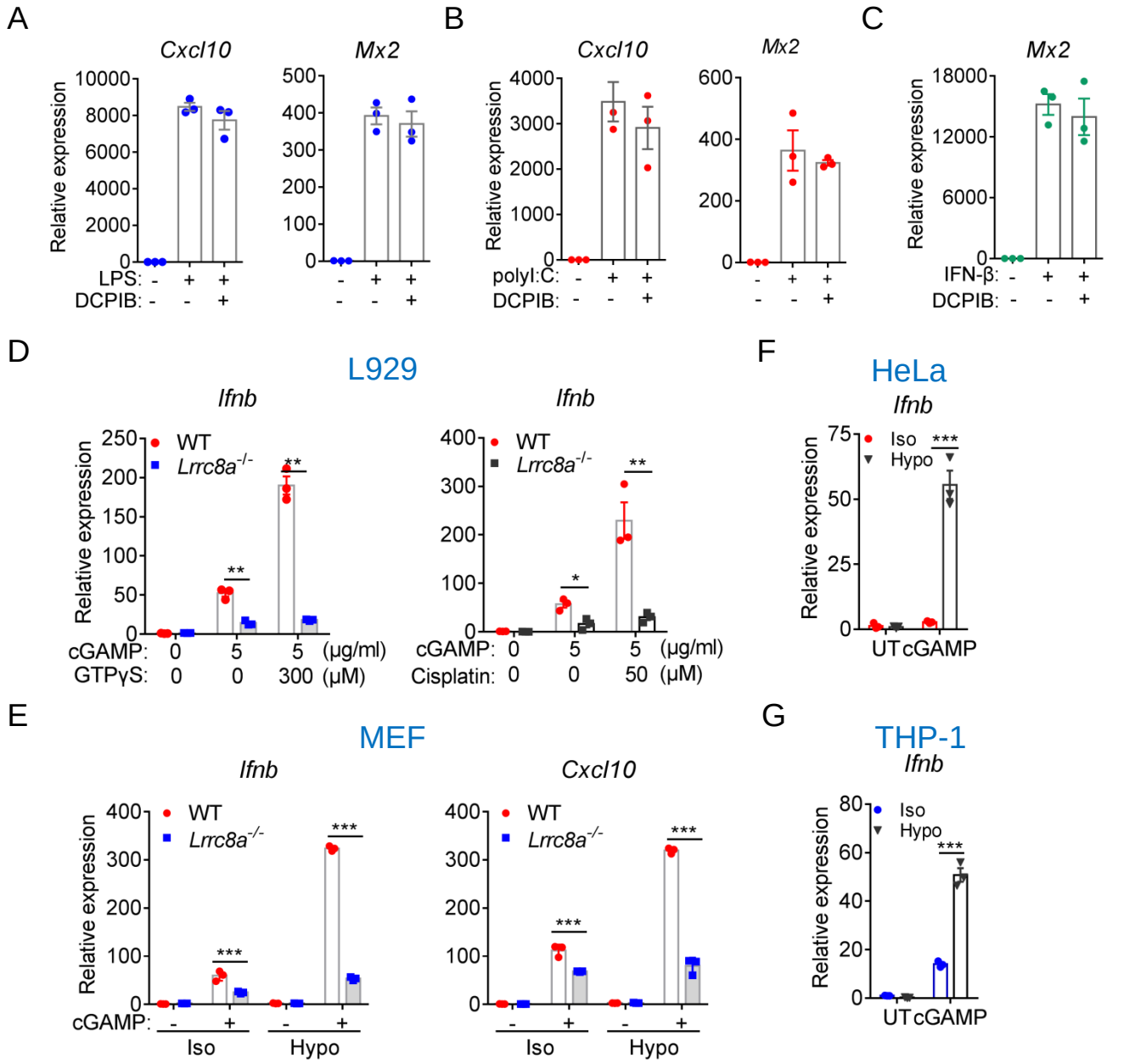

Figure S4 Lrrc8/VRAC Augments Extracellular cGAMP Responses, Related to Figure 4

(**A, B**) peritoneal macrophages were stimulated with 100 ng/ml LPS (**A**) or transfected poly I:C (1 μg/ml) (**B**) for 3 h w or w/o 20 μM DCPIB. The induction of *Cxcl10* and *Mx2* was analyzed by RT-PCR (n=3 biological replicates).

(**C**) L929 cells were stimulated by IFN-β (200 U/ml) for 3 h w or w/o 20 μM DCPIB. The induction of *Mx2* was analyzed by RT-PCR (n=3 biological replicates).

(**D**) WT and *Lrrc8a*$^{-/-}$ L929 cells were stimulated with 5 μg/ml cGAMP for 12 h in the absence or presence of GTPγS or cisplatin. The expression of *Ifnb* was measured by RT-PCR (n=3 biological replicates).

(**E-G**) MEFs (**E**), HeLa (**F**) or PMA-differentiated THP-1 cells (**G**) under isotonic or hypotonic conditions were stimulated with 5 μg/ml cGAMP for 3 h, gene expression was measured by RT-PCR (n=3 biological replicates).

Data are presented as mean ± SEM (**p<0.01, ***p<0.001, analyzed by Student's *t* test). UT: untreated.

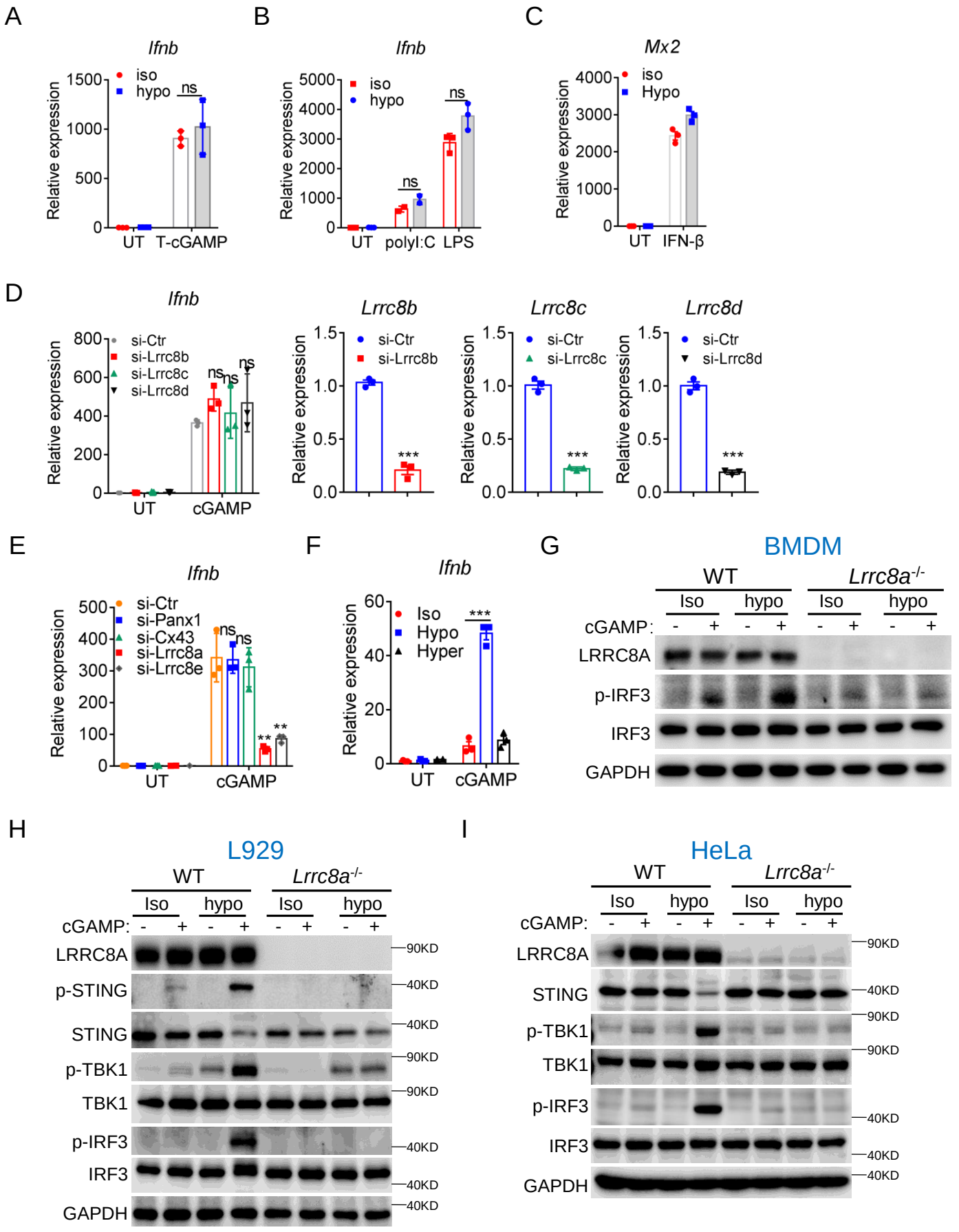
A
Ifnb
Relative expression
iso
hypo
ns
UT
T-cGAMP
B
Ifnb
iso
hypo
ns
ns
UT
polyI:C
LPS
C
Mx2
iso
Hypo
UT
IFN-β
D
Ifnb
si-Ctr
si-Lrrc8b
si-Lrrc8c
si-Lrrc8d
UT
cGAMP
Lrrc8b
Lrrc8c
Lrrc8d
***
E
Ifnb
si-Ctr
si-Panx1
si-Cx43
si-Lrrc8a
si-Lrrc8e
**
F
Ifnb
Iso
Hypo
Hyper
***
G
BMDM
WT
Lrrc8a-/-
Iso
hypo
cGAMP:
LRRC8A
p-IRF3
IRF3
GAPDH
H
L929
p-STING
STING
p-TBK1
TBK1
90KD
40KD
I
HeLa

Figure S5 VRAC-dependent Response to Extracellular cGAMP is Enhanced by Hypotonic Swelling, Related to Figure 5

(**A**) L929 cells under isotonic or hypotonic conditions were liposome-transfected with 2 μg/ml cGAMP for 3 h. The induction of *Ifnb* was analyzed by RT-PCR. (n=3 biological replicates)
(**B, C**) pMs under isotonic or hypotonic conditions were stimulated with LPS (100 ng/ml), polyI:C (30 μg/ml) or IFN-β (200U/ml) for 3 h, the induction of *Ifnb* or *Mx2* was analyzed by RT-PCR. (n=3 biological replicates)
(**D, E**) L929 cells transfected with control or gene-specific siRNAs for 48 h were stimulated with cGAMP (5 μg/ml) for 3 h under hypotonic challenge. The gene expression was quantified by RT-PCR (n=3 biological replicates).
(**F**) L929 cells under isotonic, hypotonic or hypertonic conditions were stimulated with cGAMP (5 μg/ml) for 3 h. The induction of *Ifnb* was analyzed by RT-PCR (n=3 biological replicates).
(**G-I**) BMDMs, L929 and HeLa cells were stimulated with added cGAMP (5 μg/ml) for 3 h under either isotonic or hypotonic condition, the signaling events were examined by immunoblotting. Data are representative of three independent experiments.
Data are presented as mean ± SEM. (** $p<0.01$, *** $p<0.001$, ns, not significant, analyzed by Student's *t* test). UT: untreated.

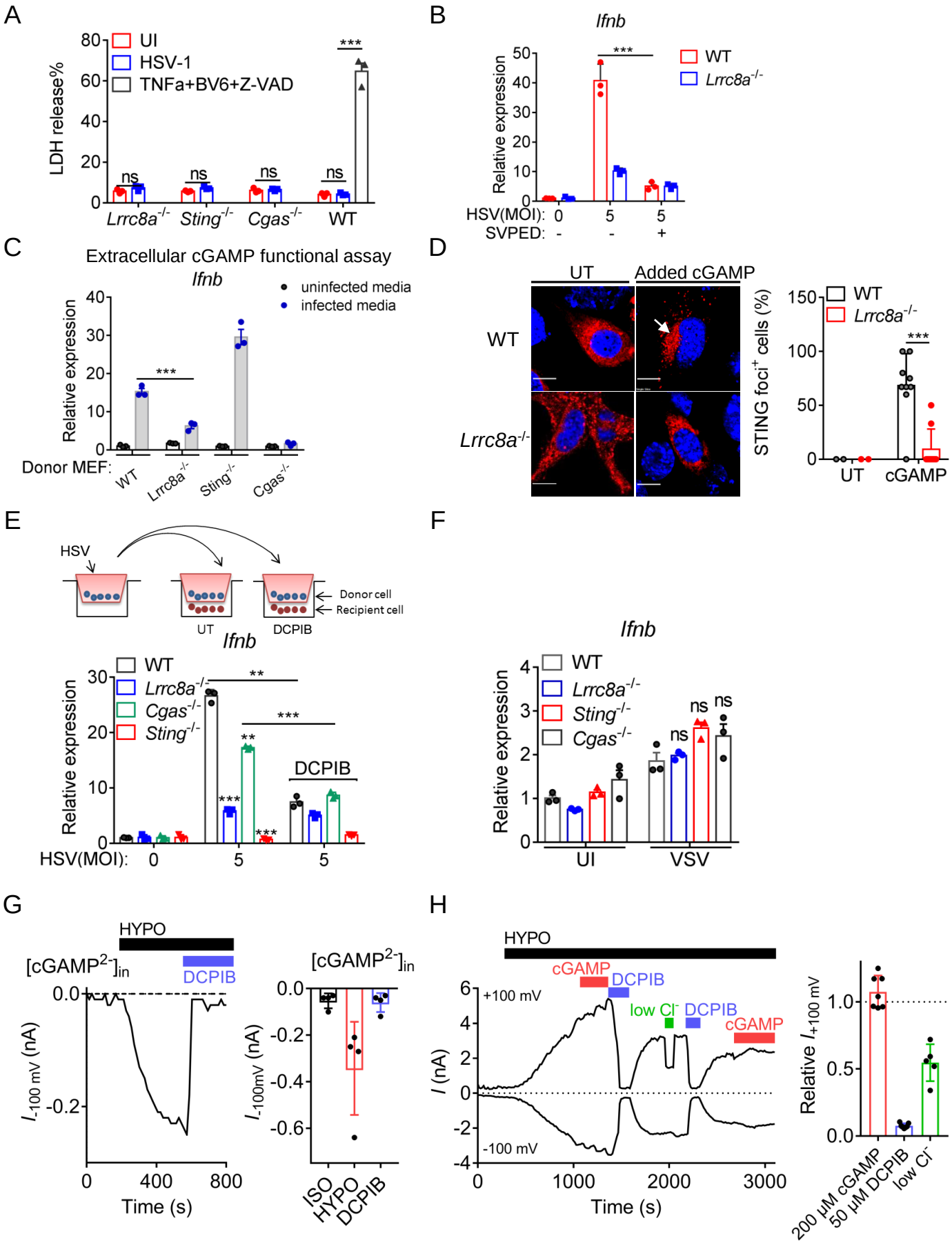
A
UI
HSV-1
TNFa+BV6+Z-VAD
LDH release%
ns
***
Lrrc8a-/-
Sting-/-
Cgas-/-
WT
B
Ifnb
Relative expression
WT
Lrrc8a-/-
HSV(MOI): 0 5 5
SVPED: - - +
C
Extracellular cGAMP functional assay
Ifnb
uninfected media
infected media
Donor MEF:
D
UT
Added cGAMP
WT
Lrrc8a-/-
STING foci+ cells (%)
cGAMP
E
HSV
Donor cell
Recipient cell
DCPIB
F
VSV
G
HYPO
[cGAMP2-]in
DCPIB
I-100 mV (nA)
Time (s)
ISO
H
cGAMP
+100 mV
-100 mV
low Cl-
I (nA)
Relative I+100 mV
200 μM cGAMP
50 μM DCPIB

Figure S6 LRRC8A/E-containing VRACs Transport cGAMP, Related to Figure 6

(**A**) MEFs were infected with HSV-1 (MOI: 5) for 6 h, and released LDH (Lactate dehydrogenase) in the media were measured by a LDH-Glo™ Cytotoxicity Assay kit. The media from MEFs treated with TNF (10 ng/ml), Smac mimetic BV6 (0.5 μM) and caspase inhibitor zVAD (20 μM) for 8 h as a positive control.
(**B**) Media from HSV-1-infected MEFs (MOI: 5, 6 h) digested with 0.5 U/ml SVPDE for 40 min were then incubated with WT or *Lrrc8a*$^{-/-}$ recipient MEFs, and *Ifnb* in recipient MEFs was analyzed by RT-PCR.
(**C**) The media from HSV-1-infected WT or gene-ablated MEFs (MOI: 5) were incubated with uninfected recipient WT MEFs for 3 h. The induction of *Ifnβ* in the recipient MEFs was analyzed by RT-PCR (n=3 biological replicates).
(**D**) WT and *Lrrc8a*$^{-/-}$ MEFs transiently transfected with plasmids expressing STING-Cherry for 18 h were untreated (UT) or treated with 5 μg/ml cGAMP without transfection for 2 h. The STING aggregates were quantified by an Image J software (n=2-8 biological replicates). Arrow indicates STING aggregates. UT: untreated.
(**E, F**) *Sting*$^{-/-}$ MEFs on a transwell chamber were infected with HSV-1 (MOI: 5) (**E**) or VSV (MOI: 0.1) **(F**) for 3 h, then co-cultured with various genotypes of recipient MLFs for 6 h w or w/o 20 μM DCPIB. The induction of *Ifnβ* in the recipient cells was analyzed by RT-PCR (n=3 biological replicates). UI: uninfected.
(G) Data from HCT116 cells patched in the whole-cell configuration with a pipette solution containing (in mM) 50 Na_2cGAMP (Invivogen), 130 mannitol, 20 EGTA, 10 HEPES, 4 MgATP, pH7.2 (NaOH). To elicit swelling-activated currents, cells were perfused with a 40% hypoosmotic bath solution containing (in mM) 82 NaCl, 6 CsCl, 1 $MgCl_2$, 1.5 $CaCl_2$, 10 glucose, 10 HEPES, pH 7.4 (NaOH), 200 mOsm/kg. 50 μM DCPIB was used. Left, representative time course of currents (at -100 mV); right, currents at -100 mV. Because VRAC activation was monitored using a ramp protocol from -100 to +100 mV and chloride was present on the extracellular side, a minor contribution by chloride loaded during the ramp to the outward current cannot be excluded.
(H) While 50 μM DCPIB potently blocked VRAC currents and a low chloride solution induced a shift in the reversal potential, no effect of 200 μM cGAMP was observed. The recording pipette contained (in mM) 140 CsCl, 20 EGTA, 10 HEPES, 4 MgATP, pH 7.2 (CsOH), 300 mOsm/kg. Na_2cGAMP (Invivogen) was solubilized in the hypotonic recording solution on the day of experiments. Application of 200 μM cGAMP was performed locally using the BioPen™ (Fluicell). To control for efficient solution delivery with this device, 50 μM DCPIB and a solution in which glutamate was substituted for chloride (low Cl^-) were applied. Left, representative time course of currents (-100 and +100 mV). cGAMP, 200 μM; DCPIB, 50 μM. Right, current relative to hypotonic control conditions.

Data are presented as mean ± SEM. (** $p<0.01$, *** $p<0.001$; ns: not significant, analyzed by Student's t test).

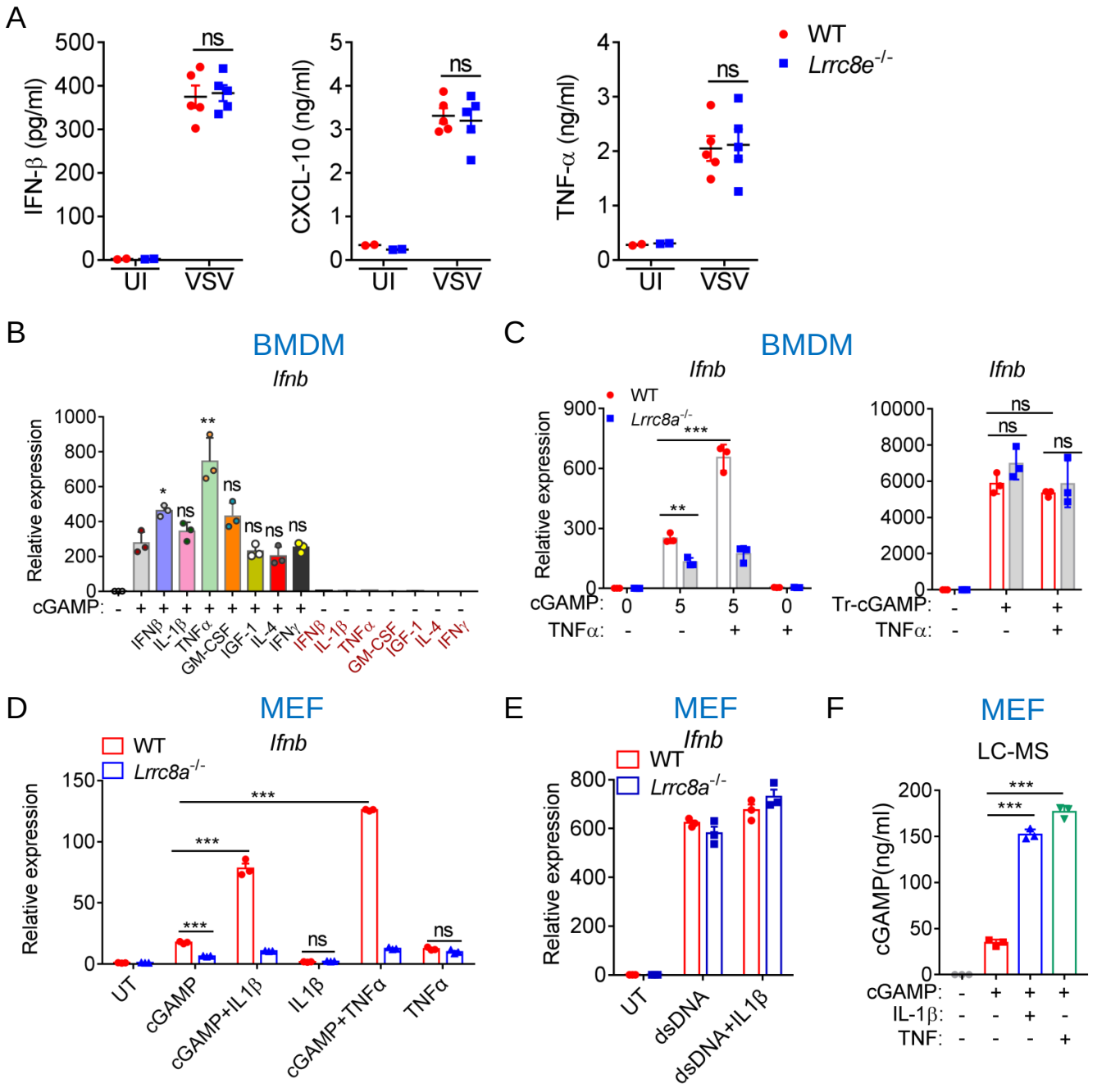

Figure S7 Proinflammatory Cytokines Enhance VRAC Activity and Bystander IFN Response, Related to Figure 7

(**A**) 8-week-old WT and *Lrrc8e*$^{-/-}$ littermates (n=5 mice) were intravenously infected with VSV (5×10^6 pfu/mouse). Sera were collected 24 h after infection for ELISA. UI: uninfected.

(**B**) BMDMs were treated with cGAMP (5 μg/ml) for 6 h w or w/o cytokine as indicated, and RT-PCR was conducted to assess *Ifnb* expression (n=3 technical replicates).

(**C**) BMDMs were treated with cGAMP (5 μg/ml) or liposome-transfected (Tr-cGAMP) 2 μg/ml cGAMP for 6 h, and RT-PCR was conducted to assess *Ifnb* expression (n=3 biological replicates).

(**D, E**) MEFs were treated with cGAMP (5 μg/ml) (**D**) or transfected 1μg DNA (**E**) w or w/o 20 ng/ml IL-1β or 20 ng/ml TNF for 3 h, and RT-PCR was conducted to assess *Ifnb* expression (n=3 biological replicates). UT: untreated.

(**F**) MEFs were treated with 5 μg/ml of cGAMP w or w/o 20 ng/ml IL-1β or TNF for 1 h in serum-free media, and cytosolic cGAMP was measured by LC-MS (n=3 biological replicates).

Data are presented as mean ± SEM. (*<0.05, ** p<0.01, *** p<0.001; ns: not significant, analyzed by Student's t test).

Table S1. Oligonucleotides Used in This Paper, Related to STAR METHODS.

Name	Sequence (5'->3')
sgRNA oligos for gene deletion of mice	
Lrrc8b-sgRNA-F	GAACGACCTCCACCGGCAG
Lrrc8b-sgRNA-R	CTGCCGGTGGAGGTCGTTC
Lrrc8c-sgRNA-F	CTACGAGCGAGCCCTCCAC
Lrrc8c-sgRNA-R	GTGGAGGGCTCGCTCGTAG
Lrrc8d-sgRNA-F	CAACTTACCAAAGATCAGG
Lrrc8d-sgRNA-R	CCTGATCTTTGGTAAGTTG
Lrrc8e-sgRNA1-F	CCGGGGTGTGCCCCCCTAC
Lrrc8e-sgRNA1-R	GTAGGGGGGCACACCCCGG
Lrrc8e-sgRNA2-F	TGGAAATCCCACTCCCATAT
Lrrc8e-sgRNA2-R	ATATGGGAGTGGGATTTCCA
siRNA oligos	
Lrrc8a-siRNA-1-F	GCUACACCGUCUACUAUGUTT
Lrrc8a-siRNA-1-R	ACAUAGUAGACGGUGUAGCTT
Lrrc8a-siRNA-2-F	CUCACUCCAUCUUUAGCCUTT
Lrrc8a-siRNA-2-R	AGGCUAAAGAUGGAGUGAGTT
Lrrc8b-siRNA-F	CUACACUACUUGGAUCUAATT
Lrrc8b-siRNA-R	UUAGAUCCAAGUAGUGUAGTT
Lrrc8c-siRNA-F	GCUGAUGAUCGGAGUGUUUTT
Lrrc8c-siRNA-R	AAACACUCCGAUCAUCAGCTT
Lrrc8d-siRNA-F	CUCAGAUGCUUAGACGUCATT
Lrrc8d-siRNA-R	UGACGUCUAAGCAUCUGAGTT
Lrrc8e-siRNA-1-F	GCUGACACAGAGGCCUUUATT
Lrrc8e-siRNA-1-R	UAAAGGCCUCUGUGUCAGCTT
Lrrc8e-siRNA-2-F	GGAGGAGGCGUGAAAGGUUTT
Lrrc8e-siRNA-2-R	AACCUUUCACGCCUCCUCCTT
hLRRC8A-siRNA-F	GCUUGCCUCUUCAGUAUUUTT
hLRRC8A-siRNA-R	AAAUACUGAAGAGGCAAGCTT
Panx1-siRNA-F	CCACUUGGCCACGGAGUAUTT
Panx1-siRNA-R	AUACUCCGUGGCCAAGUGGTT
Cx43-siRNA-F	CUGGGUCCUUCAGAUCAUATT
Cx43-siRNA-R	UAUGAUCUGAAGGACCCAGTT
sgRNA oligos for gene deletion of L929 cells	
Lrrc8a-sgRNA1-F	CACCGCATACCGGATCCTGAAGCCT
Lrrc8a-sgRNA1-R	AAACAGGCTTCAGGATCCGGTATGC
Lrrc8a-sgRNA2-F	CACCGAGGGACGCTGCAAGTCACCC
Lrrc8a-sgRNA2-R	AAACGGGTGACTTGCAGCGTCCCTC
Lrrc8e-sgRNA-F	CACCGAGCTTTTGGTTCAAATTCCC
Lrrc8e-sgRNA-R	AAACGGGAATTTGAACCAAAAGCTC
qPCR Primers	
Lrrc8a-F	CCTCCTGCAGAACCTCCAGAAC

Lrrc8a-R	GCAGCGACTGCAGTACATTGTT
Lrrc8b-F	GCAGTACTTTGCTGTGACCAACA
Lrrc8b-R	CACCAGAGGGGACAAATCTGTTA
Lrrc8c-F	GATCATCTGCCTTCCGAAAAGA
Lrrc8c-R	GTTGGTCGGTGAGGGTTTAGGT
Lrrc8d-F	TCCCGCCTCCGCCTAAG
Lrrc8d-R	TGCGACGCGAGACTTCA
Lrrc8e-F	TCAAACCCTGGTGGGATGTTC
Lrrc8e-R	TTCGTGGCTAGGCAAGCAGAT
Il6-F	AGATAAGCTGGAGTCACAGAAGGAG
Il6-R	CGCACTAGGTTTGCCGAGTAG
Cxcl10-F	CTCATCCTGCTGGGTCTGAGT
Cxcl10-R	CCTATGGCCCTCATTCTCACTG
Gapdh-F	TGGAGAAACCTGCCAAGTATGA
Gapdh-R	CTGTTGAAGTCGCAGGAGACAA
Tnfa-F	GTCCCCAAAGGGATGAGAAGTT
Tnfa-R	GTTTGCTACGACGTGGGCTACA
Ifnb-F	GCACTGGGTGGAATGAGACTATTG
Ifnb-R	TTCTGAGGCATCAACTGACAGGTC
Mx2-F	GTGCGGCCCTGCATTGACCT
Mx2-R	GGCCACTCCAGACAGTGCTTCTAGT
Cx43-F	TTCATGCTGGTGGTGTCCTTGG
Cx43-R	GCAGTCTTTGGATGGGCTCAG
Panx1-F	ATCCTGCCCACCTTCGATGTTC
Panx1-R	TCCAGCACCTTCAGACACTTGT
hGAPDH-F	CACCAGGTGGTCTCCTCTGACT
hGAPDH-R	CCCTGTTGCTGTAGCCAAATTC
hIFNB-F	AGCTGAAGCAGTTCCAGAAG
hIFNB-R	AGTCTCATTCCAGCCAGTGC
hCXCL10-F	GTGGCATTCAAGGAGTACCTC
hCXCL10-R	TGATGGCCTTCGATTCTGGATT
hIL6-F	CAGACAGCCACTCACCTCTTCA
hIL6-R	CCTCTTTGCTGCTTTCACACAT